

University of Kentucky

UKnowledge

---

Theses and Dissertations--Electrical and  
Computer Engineering

Electrical and Computer Engineering

---

2018

## PARAMETERS AFFECTING THE RESISTIVITY OF LP-EBID DEPOSITED COPPER NANOWIRES

Gabriel Smith

*University of Kentucky*, gwsm222@g.uky.edu

Digital Object Identifier: <https://doi.org/10.13023/ETD.2018.120>

[Right click to open a feedback form in a new tab to let us know how this document benefits you.](#)

### Recommended Citation

Smith, Gabriel, "PARAMETERS AFFECTING THE RESISTIVITY OF LP-EBID DEPOSITED COPPER NANOWIRES" (2018). *Theses and Dissertations--Electrical and Computer Engineering*. 114.  
[https://uknowledge.uky.edu/ece\\_etds/114](https://uknowledge.uky.edu/ece_etds/114)

This Master's Thesis is brought to you for free and open access by the Electrical and Computer Engineering at UKnowledge. It has been accepted for inclusion in Theses and Dissertations--Electrical and Computer Engineering by an authorized administrator of UKnowledge. For more information, please contact [UKnowledge@lsv.uky.edu](mailto:UKnowledge@lsv.uky.edu).

## **STUDENT AGREEMENT:**

I represent that my thesis or dissertation and abstract are my original work. Proper attribution has been given to all outside sources. I understand that I am solely responsible for obtaining any needed copyright permissions. I have obtained needed written permission statement(s) from the owner(s) of each third-party copyrighted matter to be included in my work, allowing electronic distribution (if such use is not permitted by the fair use doctrine) which will be submitted to UKnowledge as Additional File.

I hereby grant to The University of Kentucky and its agents the irrevocable, non-exclusive, and royalty-free license to archive and make accessible my work in whole or in part in all forms of media, now or hereafter known. I agree that the document mentioned above may be made available immediately for worldwide access unless an embargo applies.

I retain all other ownership rights to the copyright of my work. I also retain the right to use in future works (such as articles or books) all or part of my work. I understand that I am free to register the copyright to my work.

## **REVIEW, APPROVAL AND ACCEPTANCE**

The document mentioned above has been reviewed and accepted by the student's advisor, on behalf of the advisory committee, and by the Director of Graduate Studies (DGS), on behalf of the program; we verify that this is the final, approved version of the student's thesis including all changes required by the advisory committee. The undersigned agree to abide by the statements above.

Gabriel Smith, Student

Dr. J. Todd Hastings, Major Professor

Dr. Caicheng Lu, Director of Graduate Studies

PARAMETERS AFFECTING THE RESISTIVITY OF LP-EBID DEPOSITED COPPER  
NANOWIRES

---

THESIS

---

A thesis submitted in partial fulfillment of the  
requirements for the degree of Master of Science in  
Electrical Engineering in the College of Engineering  
at the University of Kentucky

By: Gabriel Smith

Lexington, Kentucky

Director: Dr. J. Todd Hastings, Professor of  
Electrical Engineering

Lexington, Kentucky

2018

Copyright © Gabriel Smith 2018

## ABSTRACT OF THESIS

### PARAMETERS AFFECTING THE RESISTIVITY OF LP-EBID DEPOSITED COPPER NANOWIRES

Electron Beam Induced Deposition (EBID) is a direct write fabrication process with applications in circuit edit and debug, mask repair, and rapid prototyping. However, it suffers from significant drawbacks, most notably low purity. Work over the last several years has demonstrated that deposition from bulk liquid precursors, rather than organometallic gaseous precursors, results in high purity deposits of low resistivity (LP-EBID). In this work, it is shown that the deposits resulting from LP-EBID are only highly conductive when deposited at line doses below  $25\mu\text{C}/\text{cm}$ . When the dose exceeds this value, the resulting structure is highly porous providing a poor conductive pathway. It is also shown that beam current has no significant effect on the resistivity of the deposits. Nanowires with resistivity significantly lower than the previous best result of  $67\mu\Omega\cdot\text{cm}$  were achieved, with the lowest resistivity being only  $6.58\mu\Omega\cdot\text{cm}$ , only a factor of 4 higher than that bulk copper of  $1.7\mu\Omega\cdot\text{cm}$ .

**KEYWORDS:** Liquid Phase Electron Beam Induced Deposition, Copper Resistivity, Electron Beam Lithography, Annealing, Copper Nanowires

Gabriel Smith  
4/19/17

PARAMETERS AFFECTING THE RESISTIVITY OF LP-EBID  
DEPOSITED COPPER NANOWIRES

By  
Gabriel Smith

J. Todd Hastings  
Director of Thesis

Caicheng Lu  
Director of Graduate Studies

4/19/18

## Acknowledgements

First and foremost, I would like to thank my advisor, Dr. J. Todd. Hastings, for his encouragement, patience, and invaluable advice throughout this project. Secondly, I would like to thank the other members of his research group, Sarah Lami, Mansoor Sultan, and Samaneh Esfandiarpour, for their advice, technical assistance, and scheduling flexibility as I neared the end of my thesis. I would also like to thank Dr. Joseph Elias for technical advice, providing circuit edit samples, and access to equipment at Cypress Semiconductor.

## Table of Contents

Acknowledgements.....	iii
List of Figures.....	vi
List of Tables.....	vii
1: Introduction.....	1
1.1 Current Technology Overview.....	1
1.2 Chapter Overview.....	3
2: EBID Background.....	5
2.1: EBID Overview.....	5
2.2: Introduction to LP-EBID.....	7
2.3: Previous work by this group.....	12
2.4: Advantages/Disadvantages of LP-EBID.....	15
3: Copper Background.....	18
3.1: Applications and Material Properties of Copper.....	18
3.2: Previous Copper work in EBID.....	19
3.3: Grains and Resistivity.....	20
3.4: Post Processing.....	21
4: Experimental Procedure.....	23
4.1: Materials Used.....	23
4.2: General Experimental Procedure.....	26
4.3: Experimental Parameters Investigated.....	29
4.3A: Dose.....	30
4.3B: Dose/Loop.....	31
4.3C: Current.....	31
4.4A: Annealing.....	32
4.4: Annealing Parameters.....	33
4.5: Cross Section Procedure.....	33
4.6: Resistance Measurement.....	33
5: Results.....	36
5.1: Early Circuit Edit Work.....	36
5.2: Effect of Dose.....	39
5.3: Effect of Beam Current.....	44
5.4: Effect of Annealing.....	47
5.5: Sample Degradation Over Time.....	48
5.6: Discussion.....	52
5.6A: Effect of Dose.....	52
5.6B: Effect of Current.....	54
6: Conclusion.....	56
6.1: Future Work.....	56
6.1A: Liquid Control.....	56
6.1B: Collateral Deposition Reduction.....	56

6.1C: Further Parametric Investigation.....	57
6.1D: Circuit Edit Applications .....	58
6.2: Conclusion .....	58
References.....	60
Vita.....	63

## List of Figures

Figure 1: Electron Beam Induced Deposition from a Gaseous Precursor, courtesy of Matthew Bresin.....	5
Figure 2 Cross Section of Sealed Liquid Cell under Electron Beam; Inset: Formed Deposits [9].....	8
Figure 3 LP-EBID Technique with LIS, courtesy of Matthew Bresin.....	9
Figure 4 (A) Solid Precursor Deposited Ex-Situ (B) Hydration of Precursor in ESEM (C) Deposition via LP-EBID (D) Resulting Deposits.....	11
Figure 5 (A) Schematic Illustration of micro wells (B) 50 degree tilt view of micro wells.....	12
Figure 6 Overall 4 Point Probe Pattern.....	24
Figure 7 Working Area Where Deposition Occurred.....	24
Figure 8 General Patterning Process (A) Initial Working Site (B) LIS Positioning (C) LIS Touchdown (D) Spot Scans (E) Final Deposition.....	27
Figure 9 (A) Top Down Measurement of Deposit Dimensions (B) CCD Image of Stage Tilted for Measurement (C) Deposit at 45-degree angle.....	29
Figure 10 Four Point Probe Method [21].....	34
Figure 11 (A) Unedited Test Structure (B) Sectioned Removed via Helios Dual-Beam (C) Patch implemented via LP-EBID.....	37
Figure 12 (A) Cross Section of Deposit (B) Copper Content in Deposit.....	39
Figure 13 (A) Platinum Test Structures for Two Point Measurement (B) Patched Copper Nanowires.....	40
Figure 14: Total Dose vs Number of Patterning Loops.....	41
Figure 16 (A) Looped Sample Top Down View (B) Looped Sample Cross Section (C) Looped Sample Copper Content (D) Non-Looped Sample Top Down (E) Non-Looped Sample Cross Section (F) Non-Looped Sample Copper Content.....	43
Figure 17 (A) Nanowire patterned at 259 pA (B) Nanowire Patterned at 524 pA (C) Nanowire Patterned at 866 pA.....	44
Figure 18 Sample Resistivity vs Beam Current.....	45
Figure 19 (A) Structure 4.0-UL, Lower Resistivity (B) Structure 4.0-LR, Higher Resistivity.....	47
Figure 20 (A) Deposit before Annealing (B) Deposit After Annealing.....	48
Figure 21 (A) Sample 1 Imaged in October 2017 (B) Sample 2 Imaged in October 2017 (C) Sample 1 imaged in March 2018 (D) Sample 2 imaged in March 2018.....	49
Figure 22 Probe Lead Loss of Adhesion, Former Location of Probe Lead and Section of Copper Deposit Removed are Annotated.....	50
Figure 23 (A) Copper Sample before acid exposure (B) Copper Sample after 24 of exposure to 5M Sulfuric Acid.....	51
Figure 24 Available Paths of Precursor Replenishment.....	53
Figure 25: Probe Lead Repair Via Ion Deposition of Platinum.....	55

## List of Tables

Table 1: Results from Syam Master's Thesis [21] .....	14
Table 2: Purity Achieved Across Various Materials Via LP-EBID .....	16
Table 3 Chemical Composition of EBID Deposited Copper from Various Precursors as a Function of Flux Ratio [5] .....	20
Table 4 Pipette Pull Parameters .....	25
Table 5: Resistance Comparison of Test Structures .....	38
Table 6 Looped vs Non-Looped Copper Content.....	44
Table 7 Smith and Syam Resistivity Data .....	46

## 1: Introduction

As modern integrated circuits (ICs) continue to reduce in size and increase in complexity, the demand correspondingly increases for a technology capable of reliably performing circuit edit/debug, mask repair, and easy construction of nano/micro scale three dimensional structures allowing for rapid prototyping. The task of circuit edit and debug is currently fulfilled largely by two technologies, Focused Ion Beam (FIB) and Electron Beam Induced Deposition (EBID).

### 1.1 Current Technology Overview

Ion beam systems began as an alternative to electron beam lithography, with the advantage of significantly reduced scattering relative to electron based systems [1]. Most ion sources are gallium based, though neon and helium based systems have also been constructed, with helium having a significant advantage in resolution due to ion size [1]. A precursor gas is required for an ion beam to deposit a material, and gas assistance can greatly improve the etching process. Successful ion beam deposition has been reported for many common materials, the most commonly used are platinum and tungsten [2].

In theory, the ion beam should cause the organometallic gaseous precursor to dissociate, leaving a pure metallic deposit directly under the beam and the remaining organic components to volatilize in the chamber [2]. In practice, however, there are some drawbacks to this approach. Ion beam systems have been shown to cause significant contamination to the areas surrounding the beam, this can take the form of either deposited ions from the beam itself, or amorphous elements from the precursor gases [3].

This contamination, combined with the general harshness of the beam, can result in damage to the sample.

A greater drawback, as ICs become smaller and current densities increase, is that the purity of the deposited material is not very high. For example, augur analysis has shown the purity of FIB deposited platinum to be only 46%, while tungsten is reported higher at 75% [2]. The remainder of the material being composed of mostly carbon, with some gallium contamination from the beam and a small percentage of oxygen in both cases [2].

EBID is an alternative technique to address many of the same applications. EBID works in much the same way as a FIB system, except that the precursor gas is decomposed by an electron beam rather than an ion beam. EBID is an incredibly precise technique, capable of fabricating nanometer scale structures in many different materials [4]. Though purity is still a significant drawback, with the purity of copper only reported at a maximum of 60% for gas phase EBID [4]. As copper becomes an increasingly common material in modern ICs, it becomes ever more important to develop a technique to quickly, and accurately, deposit high purity copper.

As such, significant research effort has been placed on purifying EBID copper deposits either by researching new gaseous precursors [5], or developing novel methods of deposition that can ideally improve purity and feature size [6] [7]. One notable technique, and the focus of this work, is the use of a liquid precursor rather than a gaseous one This is known as Liquid Phase Electron Beam Induced Deposition (LP-EBID).

LP-EBID has been shown to produce copper deposits of a significantly higher purity than traditional EBID [8]. Given these positive results, LP-EBID has the potential for application in areas such as rapid IC prototyping, mask repair, and circuit edit. However, there has been little research completed as to how this increase in purity affects resistivity. Particularly, it is virtually unknown what patterning conditions lead to the most conductive structures and how factors beyond purity, such as copper grain size, may affect resistivity. As such this work details an analysis across multiple experimental variables to quantify the parameters affecting copper nanowires deposited by LP-EBID.

## 1.2 Chapter Overview

This work is divided into six chapters, the first of which being this introduction. The second chapter will focus more in depth on the topic of EBID. This will include a history and notable performance benchmarks for traditional gaseous precursor EBID. The history of LP-EBID will then be described more in depth, with a particular focus on the work previously completed by this group. Finally, a summary of the advantages and disadvantages currently faced by LP-EBID will be presented to highlight the necessity of this work.

The third chapter will focus copper and the reason for its choice as the research focus. This will include an overview of the material properties of copper, and its importance to the modern semiconductor industry. Additionally, previous deposition research related specifically to copper will be reviewed to provide context as to the specific improvements that can be made via LP-EBID. Properties affecting the resistivity

of deposited copper, will be discussed including purity, copper oxidation, and grain boundary interaction. Finally, previous work on annealing copper will be reviewed as an introduction to the annealing process completed for this work.

Chapter four will focus on the specific experimental procedure used. This will describe all materials used, as well as a general case for experimental procedure. The specific parameters varied, and their hypothesized effect on resistivity, will be explained. Additionally, the parameters used for the annealing process and their selection will be reviewed. Finally, the materials and methods of the resistivity measurement will be reviewed.

The results will be presented in the fifth chapter. This will include an analysis of the effect of each varied parameter on resistivity. The discussion section will frame these results in the context of existing work in order to better understand what these results imply about the forces affecting the resistivity of copper deposited via LP-EBID. Finally, chapter six will summarize this work and tie together the previous chapters.

## 2: EBID Background

### 2.1: EBID Overview

Electron beam induced deposition has been studied for decades, with the first report of the phenomenon coming from Steward in 1934 [9]. Initially, the deposits formed in electron optical systems were seen as contamination and called “a very insidious and prevalent source of errors” [9]. It wasn’t until the 1960s that research began to be conducted on the practical application of this contamination. In the decades since, EBID has been the topic of intensive research. This has been due to the technique’s ability to be applied to many substrates, create 3D nanostructures, its high resolution, and the lack of a mask or resist that must be used in other fabrication techniques.

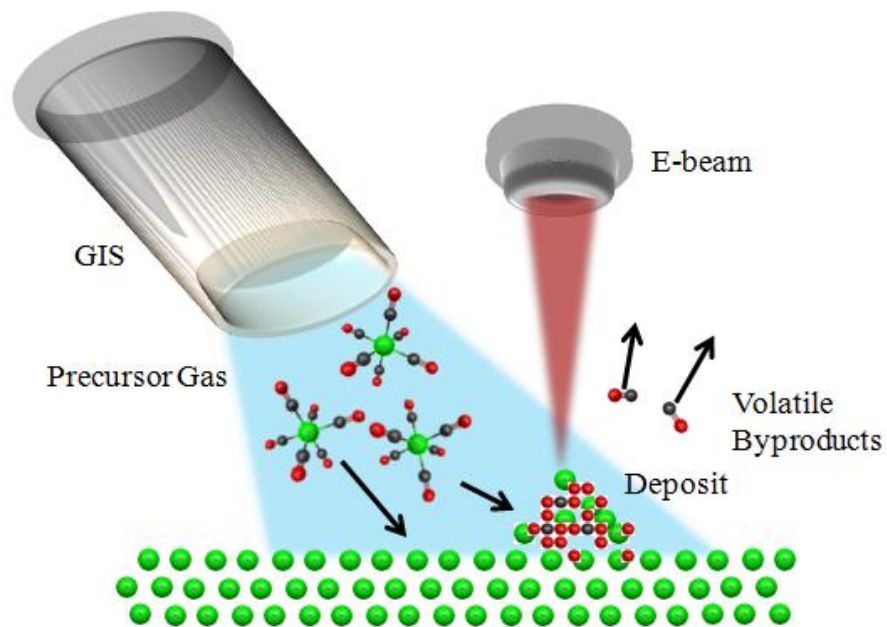


*Figure 1: Electron Beam Induced Deposition from a Gaseous Precursor, courtesy of*

*Matthew Bresin*

The traditional EBID process uses a combination of a gaseous, organometallic, precursor and an electron beam to allow for direct write patterning, functioning essentially as a localized chemical vapor deposition (CVD) process. The precursor is delivered into the chamber via the insertion of a metallic delivery needle in close proximity to the desired working area, as can be seen in Figure 1, above. The desired gaseous precursor is then pumped into the chamber from an outside reservoir. Upon exposure to the electron beam, the nonvolatile components of the precursor gas dissociate and form a deposit on the substrate. The volatile components are removed via the chamber vacuum. Though the precursor and beam parameters can greatly affect composition, the typical deposit produced via EBID consists of metallic crystals a few nanometers in size, embedded in a matrix of amorphous carbon [9].

Despite the advantages previously listed, EBID suffers from some significant drawbacks that hinder its use for several applications. Deposits are far larger than the probe size being used to fabricate them. As the structure grows, secondary electrons generated within the structure itself can cause a lateral broadening over time [10]. This imposes a limitation on the resolution of the process as the deposits will always be broader than the beam diameter.

While resolution is certainly a concern, by far the great challenge to EBID is the purity, and correspondingly, the resistivity of deposited materials. As a reference, resistivity achieved in EBID platinum deposits is  $1\ \Omega\cdot\text{cm}$  [11] and tungsten has measured at  $10^{-2}\ \Omega\cdot\text{cm}$  [12], both of these numbers being orders of magnitude higher than the bulk material resistivity. There was a clear positive correlation between resistivity and the

beam current used. Interestingly, a novel technique of depositing gold has recently achieved a resistivity of  $8.8 \mu\Omega\cdot\text{cm}$ , only four times the resistivity of bulk gold, at a purity of 91% [13]. This was achieved by using water as an oxidative enhancer during deposition to minimize the carbon contamination of the deposit. However, this method has yet to be applied to other materials, such as copper, and resistivity remains an ongoing hurdle for gas phase EBID. In contrast, LP-EBID has been shown to consistently produce deposits of a much higher purity and lower resistivity with no post processing.

## 2.2: Introduction to LP-EBID

Significant research into the LP-EBID process has not been conducted until recently. This has been due to two main issues. The primary reason for this is that the liquid film cannot be maintained with reasonable stability in a high vacuum system, which is why most LP-EBID work is conducted in an ESEM and initial work was conducted in sealed cells. Secondly, delivery and control of the liquid into the chamber has been an ongoing challenge. Three primary methods of liquid precursor delivery/control have been developed; sealed liquid cells, the use of a liquid injection system (LIS), and rehydration of precursor placed on the sample ex-situ. These will be addressed in order of first publication.

The first work using electron beam induced deposition from a liquid precursor was demonstrated by Donev and Hastings in 2009 using sealed liquid cells. [6]. This work focused on the deposition of platinum from a 1% (by weight) solution of chloroplatinic acid,  $\text{H}_2\text{PtCl}_6$ . The use of the liquid precursor proved to greatly increase

deposit purity, with the deposits reported to be comprised of 85% Pt using EDS measurements. This was higher than any previously reported purity for platinum deposits using either gaseous precursor electron beam, or ion beam systems.

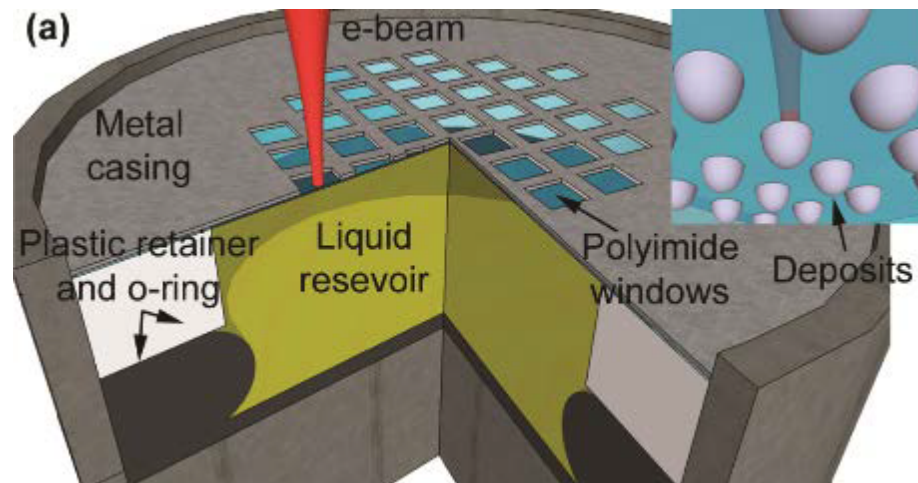


*Figure 2 Cross Section of Sealed Liquid Cell under Electron Beam; Inset: Formed Deposits [9]*

In this process, the precursor would be separated from the high vacuum chamber by a thin (150 nm) polyimide film. As can be observed in Figure 2, rectangular windows in the sealed cell allowed the electron beam to penetrate the film and form deposits on the opposite side utilizing the precursor contained in the cell. Using this method many materials have been successfully deposited using LP-EBID. In addition to the platinum previously described, these include Au [14], Ag [15], bimetallic alloys of Au and Ag [16], as well as semiconductors such as CdS [17].

However, despite the significant increase in purity observed with this technique, the use of a sealed cell proved problematic as it precluded the use of common substrates for deposition. While such experiments were useful for early investigations into LP-

EBID, the ability to deposit on common substrates such as silicon is necessary for any practical application.

The first instance of LP-EBID being used on bulk substrates was reported by Randolph, et al, in 2013 [18]. A conductively coated nano-capillary needle is used to inject the liquid precursor, in this case  $\text{CuSO}_4$ , onto the substrate. A combination of a Peltier heating/cooling stage and variable pressure allowed by operating in ESEM mode was used to control the liquid after injection.

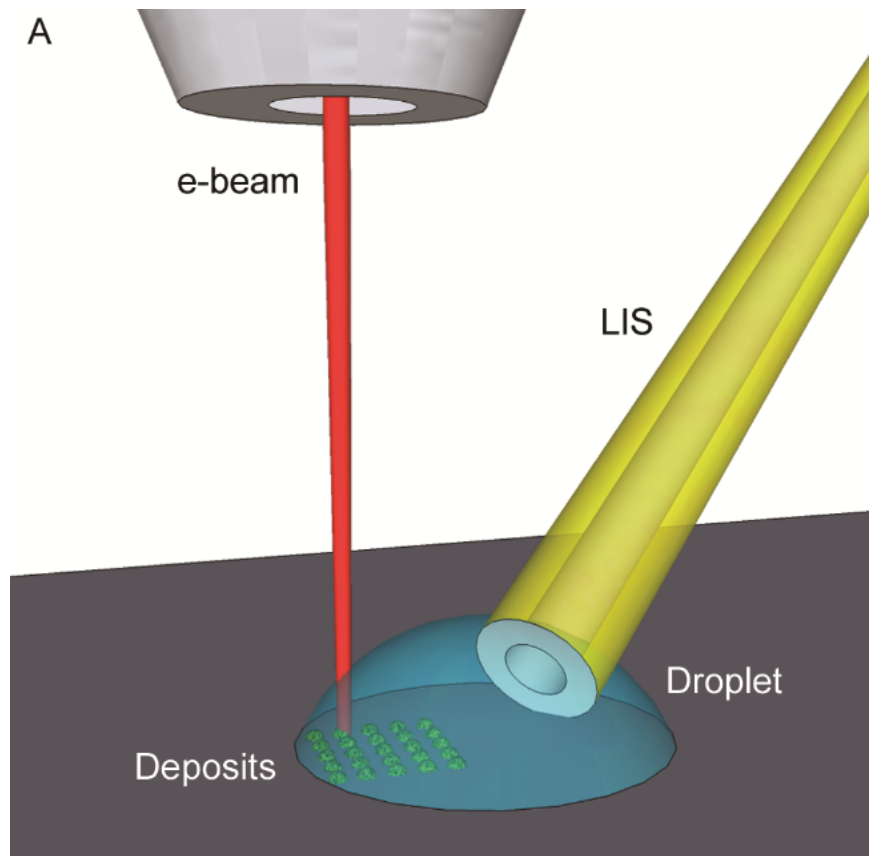


*Figure 3 LP-EBID Technique with LIS, courtesy of Matthew Bresin*

However, there were some key differences between this approach later uses of a liquid injection system for LP-EBID and that seen in Figure 3, above. Trenches were

milled into the SiO<sub>2</sub> layer of the substrate to expose the pure Si beneath it. This was accomplished using FIB in an FEI Company Quanta 3D FEG Dual Beam. This approach allowed them to determine that the deposition rate was significantly greater on the exposed Si versus the SiO<sub>2</sub> substrate. It should be noted, however, that later work has found copper deposited on an Si substrate has significant adhesion issues when removed from the vacuum chamber compared to SiO<sub>2</sub> [8].

The exposure time (2 hours) and beam current (16 nA) were both much higher than is described in later papers on copper LP-EBID [8]. Additionally, this paper, and other earlier uses of a LIS [19], biased the conductive needle during the patterning process. This created a continuous flow of liquid onto the substrate, rather than retracting the nano-capillary and leaving a droplet behind which could be manipulated via chamber pressure. [18].

An interesting variation of this technique is using the needle bias, and a low vapor pressure precursor, to nano-electrospray the substrate without making direct contact [19]. These experiments were performed in high vacuum and were a balancing act between the continuous flow of liquid into the chamber and the evaporation and liquid decomposition upon interaction with the electron beam [19].

In theory, a LIS allows for accurate point delivery of a liquid precursor with a known concentration. In practice, such a system can have some distinct disadvantages. Targeting the desired area is often difficult, as the continuous removal and reinsertion of the nano-capillary needle requires the realignment of the LIS with the electron beam for each experiment. Additionally, the risk of freezing or salt formation within the needle means that precursors must be carefully selected to ensure reliable delivery. When

conducting experiments where location targeting is not critical, the LIS is not the most advantageous delivery system. Thus, some previous research has introduced the precursor ex-situ and rehydrated it within the chamber to avoid using either sealed liquid cells or a LIS to study LP-EBID.

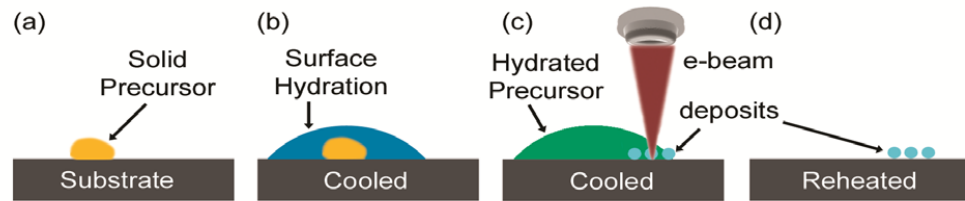


*Figure 4 (A) Solid Precursor Deposited Ex-Situ (B) Hydration of Precursor in ESEM (C) Deposition via LP-EBID (D) Resulting Deposits*

This liquid delivery method was first implemented by Bresin, et al, in 2014 [20]. In this technique, aqueous precursor solutions were placed onto the substrate and allowed to dry ex-situ, leaving behind the solid precursor seen in Figure 4(a). Once the ESEM chamber was pumped, bringing the sample to 100% relative humidity via pressure/temperature manipulation allowed for surface hydration (Figure 4(b)). Like the LIS technique, the liquid film's size and thickness could be manipulated using chamber pressure. Once the liquid film was stabilized, patterning could then be performed on the liquid edge, where the film was thinner allowing for better beam penetration (Figure 4(c)). Once the chamber was vented, the liquid film would dry up, leaving behind the desired deposits. While this technique avoids the often problematic alignment of the LIS, it does not allow for targeting specific areas for patterning and was thus not used in this

work, where all depositions had to occur on pre-patterned probe leads.

### 2.3: Previous work by this group

Prior to this work, significant research effort has been put into studying the process of LP-EBID by Dr. J. Todd Hasting's research group. Though work has been completed on other metals, the significant previous research on both copper precursors and deposition techniques has been invaluable to current efforts. In particular two previous works stand out as being heavily referenced throughout this project.

In their 2017 paper, Esfandiarpour, et al, attempt to improve the resolution and purity of copper EBID from liquids while reducing unintended deposition and avoiding precipitation of undesired products [8]. This goal was primarily pursued by modifying the liquid precursor solution, primarily composed of copper sulfate ( $\text{CuSO}_4$ ), by adding surfactants to reduce the contact angle, using additives common to electroplating baths, and reducing the organic components of the solution. The liquid precursor was applied using the rehydration method described in Section 2.2.

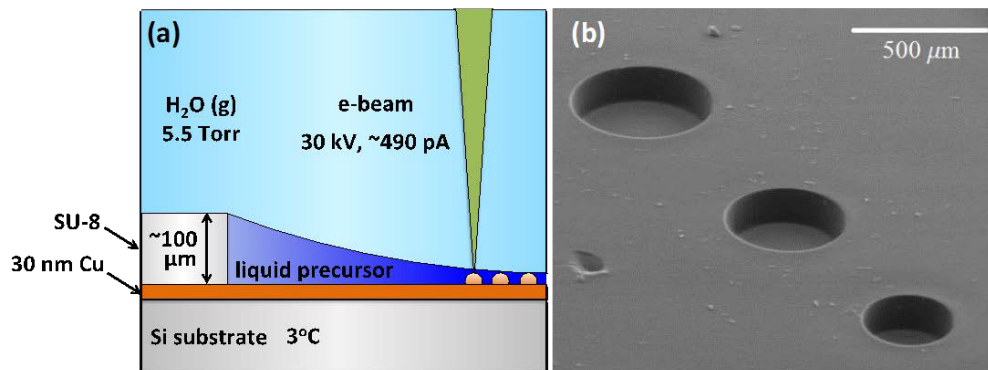


Figure 5 (A) Schematic Illustration of micro wells (B) 50 degree tilt view of micro wells

Two different surfactants were used for deposition, with the ultimate goal of significantly reducing the contact angle and allowing for a broader, more predictable, region of the liquid film for patterning. Sodium dodecyl sulfate (SDS) was added to a solution of copper sulfate, this resulted in higher resolution deposits. However, the liquid film spread so rapidly that micro wells were used to contain and control the liquid, as can be seen in Figure 5. Additionally, at the temperatures used for deposition, the SDS would precipitate as crystals on the substrate, resulting in significant collateral deposition. Though the contamination in the resulting deposit was not quantifiable via EDS measurement, significant carbon and oxygen peaks in addition to carbon indicated SDS to be sub-optimal as an additive. Due to these issues, it was replaced as an additive by another surfactant, Triton X-100. Triton X-100 has a much broader range of working temperatures and will freeze before precipitating, seemingly making it more ideal for LP-EBID [8]. However, at higher concentrations it can form an insoluble gel and, like SDS, increases oxygen contamination in deposits, also making it a sub-optimal additive.

The most promising additive was the addition of sulfuric acid ( $\text{H}_2\text{SO}_4$ ) to the precursor, resulting in a solution of 0.25 M copper sulfate and 0.1 M sulfuric acid. The low freezing point of sulfuric acid makes it ideal for working in a vacuum and maintaining a stable liquid film as chamber conditions vary. Additionally, the acid reduced the surface tension of the droplet, allowing for a broader more uniform liquid edge. Finally, the sulfuric acid significantly reduced oxygen contamination in the deposit. EDX analysis revealed that deposits from this solution were at least 88% copper, a significant improvement over previous gas based methods [8]. While other additives,

most notably PEG, were experimented with, sulfuric acid provided the most optimal combination of purity and liquid control and has thus been used in LP-EBID work that has followed.

In the spring of 2017 Amjad Syam completed a master's thesis analyzing the resistivity of copper nanowires deposited via LP-EBID [21]. The main goal of this work was to analyze the effects of the various additives described previously to the copper sulfate used for deposition of copper in LP-EBID. For these experiments, four-point probe patterns were fabricated via electron beam lithography at the University of Kentucky. The LIS method of liquid injection was used to ensure accurate delivery to the relatively small working area on the sample.

*Table 1: Results from Syam Master's Thesis [21]*

Line	Acc. voltage (kV)	Pressure (Torr)	Beam Current (pA)	Dose ( $\mu\text{C}/\text{cm}$ )	Length ( $\mu\text{m}$ )	x-sectional area ( $\mu\text{m}^2$ )	Resistance ( $\Omega$ )	<b>Resistivity (<math>\mu\Omega\cdot\text{cm}</math>)</b>
a	30	5.7	550	25	3.3	0.76	210	<b>5000</b>
b	30	5.7	550	20	2.9	0.36	63	<b>800</b>
c	30	5.5	683	20	3.6	0.36	37	<b>370</b>
d	30	5.5	1286	10 $\times$ 5 loops	3.7	0.45	5.5	<b>67</b>

The results from this thesis can be seen in Table 1, above. The lowest recorded resistivity of  $67 \mu\Omega\cdot\text{cm}$  is orders of magnitude lower than the lowest recorded resistivity obtained from gas based EBID which is  $10 \text{ k}\Omega\cdot\text{cm}$ , without a post processing step and  $1 \Omega\cdot\text{cm}$  after annealing [22]. Though these results are certainly a great improvement over previous methods, it is still far higher than the resistivity of bulk copper at  $1.7 \mu\Omega\cdot\text{cm}$ .

The materials and methods are similar enough to those presented by Esfandiarpour, et al that the purity of the nanowires can be assumed to be very high, at least above 80%. Despite the relative purity of the deposits, the resistivity of the nanowires is still a factor of 40 higher than bulk. The high purity and relatively low resistivity compared to bulk suggests that there are other factors at play in determining the resistance of LP-EBID deposited copper beyond the purity. Additionally, as can be seen in the table above, it appears that resistivity decreases with increasing beam current, but there are not enough samples to determine if this is a consistent trend. A more detailed study will be necessary to determine what factors are critical to the resistivity of copper deposited by LP-EBID and how to optimize deposition quality.

#### 2.4: Advantages/Disadvantages of LP-EBID

The greatest advantage LP-EBID has over previous techniques is its purity. As can be seen in Table 2, below, LP-EBID has been able to consistently demonstrate a higher purity across many common materials. It should be noted that all quoted purity values are in absence of any post processing steps. Furthermore, the gas-phase purity values below are not at all typical. Standard processes often yield far less than 50 at% in laboratory environments, and copper is one of the most difficult materials to deposit with high purity. Though for many materials work has yet to be completed on the resistivity of LP-EBID deposited structures, based on previous work it has been shown to correlate with purity. In addition, the technique allows for the deposition of materials that have no

known gaseous precursor, as well as providing lower cost, non-toxic, and safer alternatives to the often dangerous and expensive gases required for EBID.

*Table 2: Purity Achieved Across Various Materials Via LP-EBID*

Material	Gas Phase Purity	Liquid Phase Purity	References
<b>Copper</b>	60%	88%	[5] , [8]
<b>Platinum</b>	83%	85%	[4] [6]
<b>Silver</b>	N/A	85%	[15]
<b>Gold</b>	91%	>95%	[13], [14]

Though the advances in purity are a remarkable advantage for LP-EBID, the technique suffers from several drawbacks. Most prominent among these is a lack of repeatability due to poor liquid control. Though the use of an LIS and manipulation of chamber temperature and pressure allow for indirect control of the liquid film, it is still an inexact process to achieve and maintain a good thickness for patterning. This is especially true if the patterning must be performed in a specific working area, rather than in any ideal location along the droplet edge. Though there have been efforts to increase the area suitable for patterning, such as the use of surfactants by Esfandiarpour, et al, the ideal region remains a relatively small border on the edge of the liquid droplet. Due to this issue, the technique remains far less accurate and reliable than EBID using a gaseous precursor and currently prevents the creation of very large or complex structures.

Though liquid control is certainly the most pressing issue, more work is required to better quantify exactly how resistive the deposits produced by the technique all. While Syam presented low resistivity nanowires, they were still significantly higher than bulk and there was insufficient data to conclude what effect any patterning conditions had on the process. In order to use LP-EBID in any practical application the resistivity must be confirmed to be reliably low and the ideal patterning conditions to achieve low resistivity deposits must be found. In order to achieve this, it becomes critical to identify any factors at play in determining resistivity beyond simply the purity of the deposit.

### 3: Copper Background

#### 3.1: Applications and Material Properties of Copper

Since its inception, the semiconductor industry has been driven by improvements to device density and performance over time. In general, device performance is improved as gate length, dielectric thickness, and junction depth are scaled [23]. However, scaling down the size also reduced the area of the metallic interconnects, which increases their resistance due to decreased cross-sectional area. Though aluminum was the dominant interconnect material, the need for lower resistance has driven the adoption of copper for use in interconnects in VLSI circuits.

Copper's primary benefit over aluminum is the decreased resistivity. For reference, the resistivity of bulk aluminum is  $2.65 \times 10^{-8} \Omega \cdot \text{m}$  compared to copper's bulk resistivity of  $1.68 \times 10^{-8} \Omega \cdot \text{m}$ . This is a relative comparison, as these values can change significantly depending on the method of deposition and the size of the structure. Copper also suffers from less electromigration than aluminum. Electromigration occurs when the momentum of electrons within an electric field is transferred to lattice bound ions, and can result in a break in connection over time. This results in copper interconnects having a median lifetime 1-2 orders of magnitude greater than that of aluminum [24]. However, unlike aluminum, the oxidation of copper is not self-limiting, which can lead to increased contact resistance [25].

### 3.2: Previous Copper work in EBID

The economic importance and numerous applications of a reliable method to direct write copper has resulted in previous research efforts to deposit conductive copper structures via gas based EBID. Most precursors used are organic materials, wherein the copper is bonded to complex molecules of hydrogen, oxygen, and carbon. Precursors used also have low vapor pressure, which is necessary to work in a high vacuum SEM environment. Using EBID copper deposits can be achieved in a precise location relatively easily. However, due primarily to ligand decomposition such deposits suffer from massive carbon contamination and are typically less than 20% copper by atomic percent [26].

In an attempt to overcome this drawback, a range of precursors have been experimented with for deposition. These gases differ greatly in vapor pressure, which determines the precursor molecule flux for focused electron beam deposition [5]. They also differ in the more difficult to quantify trait of chemical stability. Chemical stability is primarily determined by dissociation temperature of the ligands, which itself is determined by thermogravimetry and the CVD temperature. The initial deposition rate correlates with precursor flux, but then decays over time inversely correlated to this initial value [5]. In general, it has been found that the purity of these deposits correlates to the electron/precursor flux ratio and the precursor stability [5]. Table ,3 below, illustrates this trend for several organometallic precursors. However, a wide array of variability can be observed.

*Table 3 Chemical Composition of EBID Deposited Copper from Various Precursors as a Function of Flux Ratio [5]*

Precursor	Cu at%	Flux Ratio (e/molecule)
Cu(hfac) <sub>2</sub>	14	1500
(hfac)CuMHY	13	55
(hfac)CuVTMS	20-45	28
(hfac)CuDMB	25-60	2

### 3.3: Grains and Resistivity

There are other factors at play in determining the resistivity, and therefore ultimate usefulness of EBID deposited copper beyond the purity. One of the more interesting, and potentially impactful, of these is the grain boundary interaction. The internal geometry of copper, from any deposition method, is non-uniform. Pure metal is concentrated in grains which are separated by grain boundaries which have a high concentration of impurities [27]. These boundaries have been found to play a significant role in determining the resistivity of the material.

The decreasing line width of Cu interconnects in progressive USLI designs comes with increasing resistance and a larger RC delay due to electron scattering [28]. Grain boundaries specifically have been found to account for at least a quarter of this scattering effect [29]. Experimentally it has been shown that larger grains correlate with a lower resistivity [28]. The smaller the copper grains, the boundaries occur, and thus more scattering creates a higher resistivity. Thus many post processing techniques center on the coarsening of the copper grains.

### 3.4: Post Processing

Annealing is the heating a material with the purpose of altering its microstructure. In the case of copper, this has the goal of coarsening the grains and burning off impurities, which decreases material resistivity. Typically, this is done thermally in an annealing furnace, though the annealing effects of hot plates, lasers, and transmission electron microscopes have also been studied for EBID deposits [30].

A study by Chnag, et al, on highly pure electroplated copper have revealed that significant gains in conductivity result from higher annealing temperatures over a shorter time, however very high temperatures have the drawback of damaging IC insulator layers or barrier metals [31]. It has been illustrated that a high heating rate, with a lower final temperature, can produce a greater reduction in resistivity than traditional annealing processes [32]. Using a temperature 100 K lower than a typical process, 573 vs 673 K, and a process time a third of the length, 10 vs 30 minutes, resistivity of electroplated copper was decreased an additional 16% compared to traditional annealing processes [32]. It was proposed that the low heating rate condition releases more grain boundary energy reaching the final temperature, leaving less energy to coarsen the grains in the isothermal stage, while the high rate conserved this energy allowing for courser grains to be achieved and thus a lower resistivity.

Annealing of EBID deposited copper from precursors of  $\text{Cu(II)(hfac)}_2$ ,  $(\text{hfac})\text{Cu(I)(VTMS)}$ , and  $(\text{hfac})\text{Cu(I)(DMB)}$ , did not result in significant metal grains, and did cause in a 70% loss in volume due to the large amount of impurities removed by the

process [30]. The resistivity was improved by an order of magnitude, from  $10 \text{ k}\Omega\cdot\text{cm}$  to  $1 \text{ k}\Omega\cdot\text{cm}$ , however this remains many orders of magnitude above that of bulk copper [30]. With the previously described low purities of copper deposited via EBID, any improvement in resistivity from annealing can be assumed to result from the removal of impurities rather than the coarsening of copper grains. There has, as of yet, been no study on the effect of annealing on copper deposited via LP-EBID.

## 4: Experimental Procedure

### 4.1: Materials Used

All deposition experiments were performed in a Quanta250 FEG Environmental Scanning Electron Microscope (ESEM), manufactured by FEI Co. Patterning was controlled by a Raith Elphy 7 electron beam patterning system. The Quanta was always operated in ESEM mode, as LP-EBID, without the use of sealed liquid cells, requires precise control of chamber conditions to maintain and manipulate the liquid film. A Peltier liquid cooling stage was used to precisely control substrate temperature. To image in ESEM mode, a gaseous secondary electron detector (GSED) was used.

The four-point probe samples, used in all resistivity experiments except the first two, were designed using Layout Editor software. After difficulties with adhesion, and measurements, on previous probe pads the size of the pads was increased to 200  $\mu\text{m}$  x 200  $\mu\text{m}$  for these experiments. The structures are composed of a 15 nm thick layer of gold with a thin chromium adhesion layer and were patterned and diced at the University of Louisville Micro/Nanofab Technology Center on a silicon substrate with a 1.7  $\mu\text{m}$   $\text{SiO}_2$  layer. This insulating layer reduces leakage current as the resistivity of deposited structures is measured. The patterns used for creating the four-point probe structures can be seen in the figures below.

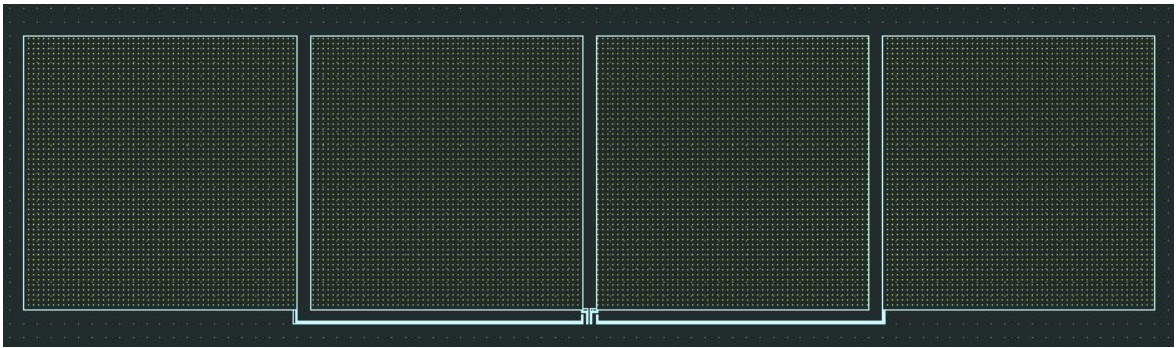


*Figure 6 Overall 4 Point Probe Pattern*

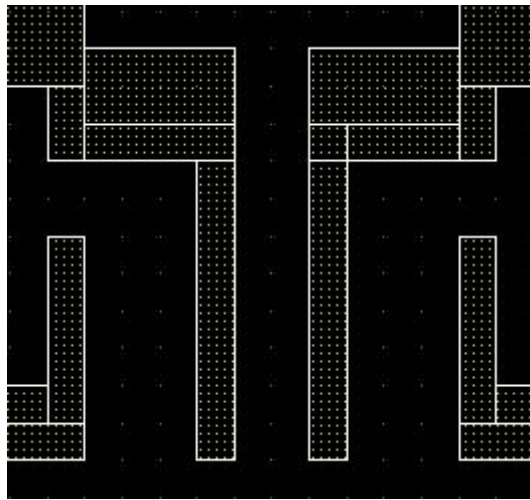


*Figure 7 Working Area Where Deposition Occurred*

As mentioned in previous sections, significant previous work has been completed on determining the ideal precursor for LP-EBID of copper. For all experiments, a two-part solution of 0.25 M Copper Sulfate  $\text{CuSO}_4 \cdot 5\text{H}_2\text{O}$  (Fisher Scientific), diluted in deionized water, and 0.1 M Sulfuric Acid  $\text{H}_2\text{SO}_4$  was used. The copper sulfate serves as the copper carrier, from which the deposits will form due to the electron beam interaction. The sulfuric acid is added as its high vapor pressure virtually eliminates any

risk of freezing in the chamber and because it significantly reduces oxygen contamination, resulting in higher purity deposits [8].

The precursor was placed on the substrate in-situ via the use of a liquid injection system (LIS) developed by FEI company (Randolph and Botman –ACS Advances). The LIS employs a nanocapillary needle that is filled with the desired precursor ex-situ, then fitted into the system before the ESEM chamber is pumped. Initially, these needles were coated with a layer of copper to reduce charging in the chamber, however for these experiments only uncoated needles were used as this significantly reduced the fabrication time. All pipettes used were fabricated on site using Sutter P-97 Flaming/Brown Micropipette Puller and 1 mm outer diameter thick walled borosilicate glass. The parameters used to pull the pipettes can be seen in Table 4, below. It should be noted that heat is a relative value and must be set according to the maximum heat of each filament.

*Table 4 Pipette Pull Parameters*

Parameter	Heat	Pressure	Delay	Pull	Velocity
Value	482	500	01	00	18

While the pipettes were initially coated to prevent charging, this process often resulted in a broken tip. All pipettes used in this work were uncoated, which resulted in a reliably unbroken tip at the cost of reduced imaging quality due to charging in the chamber. The tip diameter was determined via the pipette pull parameters and varied between approximately 0.5 and 5  $\mu\text{m}$ . The LIS allowed for precise control of where the

droplet would form on the substrate, an invaluable advantage when working with such a small area.

#### 4.2: General Experimental Procedure

Excluding the parameters that were varied, each experiment followed a general procedure. First, 10 uL of the precursor was transferred into the nanocapillary needle using a pipette. This was then fitted with a metal collar and secured into a centrifuge. The centrifuge cycle lasted 10 minutes, this ensured the precursor was concentrated at the tip of the nanocapillary needle.

During the centrifuge cycle, the Quanta chamber was prepared for ESEM mode by inserting the Peltier cooling stage and the GSED detector. The Peltier was kept at a constant temperature of 3° C in all cases. Once the centrifuge cycle completed, the LIS was fitted into the back of the Quanta chamber. A test insertion was then performed before pumping, to ensure the needle would not impact the pole piece or the GSED.

Then, a diced sample was separated from the 4-inch patterned wafer using tweezers. This sample was then rinsed for 15 seconds each in a sequence of acetone, isopropyl alcohol, and DI water and dried with compressed air. Silver paste was then applied to the bottom and along on edge of the sample. This ensured good thermal conductivity between the Peltier stage and the sample, and also served to adhere it to the stage so it would not be disturbed during the chamber pumped.

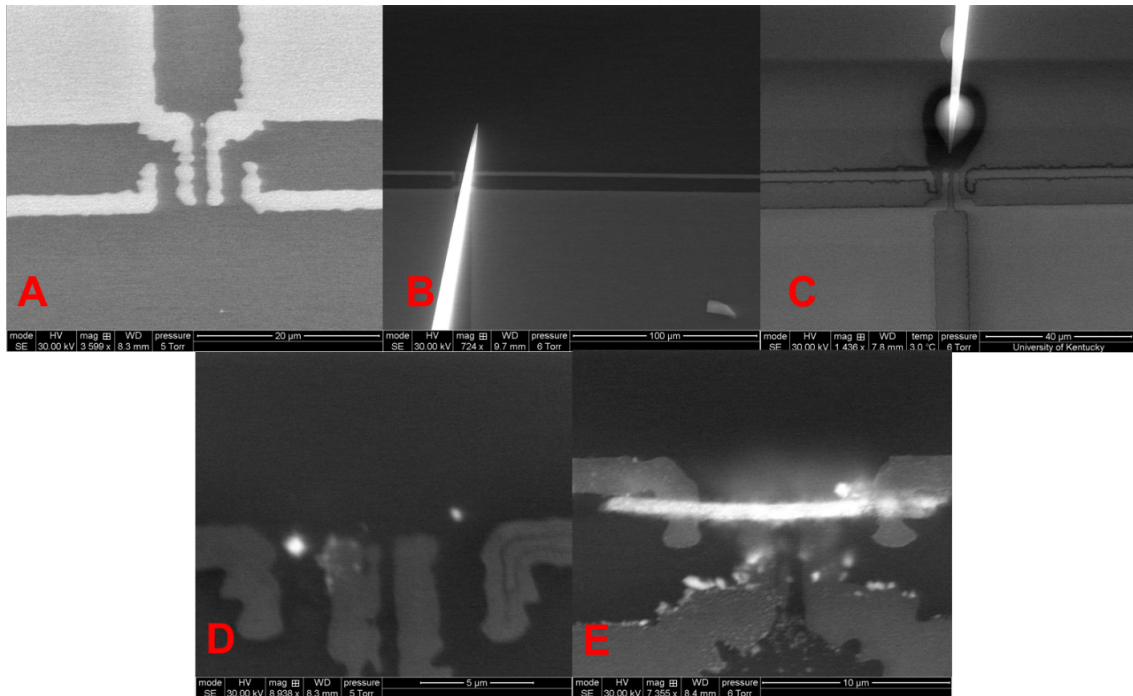


*Figure 8 General Patterning Process (A) Initial Working Site (B) LIS Positioning (C) LIS Touchdown (D) Spot Scans (E) Final Deposition*

Once the chamber was prepared and sample secured, the ESEM was then pumped directly to 5.5 torr. The process beyond this point is illustrated in Figure 8, above, and each step corresponds to the image indicated. After the image was properly focused and centered on one of the four point probes (A), the LIS could be inserted (B). As the LIS was removed between each experiment, it was often out of alignment with the center of the beam. This usually required some adjustment using screws outside the chamber to properly align the needle. The stage was lowered during this process to ensure there was no unintentional impact with the sample.

After the needle was aligned, the stage would be incrementally raised to meet it. The desired height could roughly be determined by focusing the beam on the needle, however the main indicator of contact with the sample was a slight, but visible, shift in the needle's position (C). Contact was generally far from the desired working area, so

that as the droplet expanded only the thin edge would cover it and to account for the LIS shifting forward after touchdown. Once a reasonable amount of liquid was dispensed, the LIS would be withdrawn and chamber pressure increased incrementally to 5.7 torr to expand the droplet to the desired area. Once this was achieved, the pressure would be reduced to halt further expansion.

Test spot scans were performed near the desired area, but not in the pattern's desired footprint (D). These focused the beam on a single point for several seconds. In absence of a reliable method for determining the liquid thickness, this step was necessary to verify that the area was ideal for deposition. Depending on the deposits, or lack thereof, left by the scans, the chamber pressure would be adjusted to modify the thickness of the droplet.

Once an area was determined to be suitable for patterning, beam control would be transferred to the Raith system and a horizontal line 14  $\mu\text{m}$  long would be patterned across the probe leads (E). This would then be imaged first using the GSED and again under high vacuum. Post processing included a low pressure rinse with DI water, however this was not true in all cases as significant issues were experienced with adhesion of the gold to the  $\text{SiO}_2$  substrate.

The process differed for the dose series of structures. Since these were only a test of conductivity, the structures were patterned directly between the center two pads. The slight trench between the pads served as a liquid guide. The resulting gradient of liquid thicknesses allowed for easy access to ideal patterning thickness and thus rapid fabrication of many samples.



*Figure 9 (A) Top Down Measurement of Deposit Dimensions (B) CCD Image of Stage Tilted for Measurement (C) Deposit at 45-degree angle*

The physical dimensions and location of each successful pattern were logged using high vacuum imaging to determine the resistivity after the resistance measurements were completed. As can be seen in Figure 9 (A) this was first completed top down to measure the width and length of the structure between the two inner leads. The stage was then tilted to  $45^\circ$  (B) to allow for imaging the height of the deposit (C). Basic trigonometry was then applied to compute the actual height from the substrate. The deposit was modeled as a perfect square when estimating the cross sectional area as it did not decline very gradually at the deposit edge.

#### 4.3: Experimental Parameters Investigated

There are numerous variables governing the LP-EBID process. The beam current, line dose, liquid thickness, precursor chamber conditions, dwell time, and accelerating voltage all play a role in the process. While some, such as dose, may be continuously varied others, such as beam current, can only be experimented at discrete values as determined by equipment limitations. Liquid thickness is perhaps the most critical

parameter, but due to only having indirect control of this variable via modification of chamber temperature and pressure it remains impractical to conduct a parametric study on its effect. Thus the variables chosen for experimentation were those that could both be easily controlled and were thought to have the greatest impact on the resistivity of the deposited structure.

#### 4.3A: Dose

Dose, in units of  $\mu\text{C}/\text{cm}$ , governs the total amount of charge delivered to the deposit and can be described by Equation 1, below. In the case of this work, lines are formed by progressively stepping the beam to a series of points, maintaining a constant dwell time at each to ensure the proper dose is delivered and is uniform across the structure. Given a beam current, determined by the SEM, and a desired dose the dwell time is automatically calculated to compensate. It was thought that total dose would have no effect on the final deposit beyond increasing its size, however after initial experiments revealed a strong correlation between resistivity and dose further investigation was warranted. Since earlier works established the conductivity for lower dose deposits [21], this work focused primarily on higher doses of 100 and 250  $\mu\text{C}/\text{cm}$ .

$$Dose = \frac{Beam\ Current * Dwell\ Time}{Step\ Size}$$

Equation 1: Line Pattern Dose Calculation

#### 4.3B: Dose/Loop

The total dose for any deposition can be delivered in any integer number of patterning loops. Earlier observations suggested that looping improved pattern quality, however it was initially feared that more loops would result in smaller copper grain sizes and thus a larger resistivity. So initial depositions were performed in only one loop to avoid this effect. However, like total dose, early results suggested the dose/loop had a much greater effect than previously thought. To investigate this, a constant dose of  $100 \mu\text{C}/\text{cm}$  was used with the dose split among varying numbers of loops. The total dose was also varied with the dose/loop remaining constant to isolate any results to dose/loop rather than simply total dose. Additionally, cross sections were performed at  $100 \mu\text{C}/\text{cm}$  /loop and  $20 \mu\text{C}/\text{cm}$  /loop, with the same total dose, to check for any variation in internal deposit geometry.

#### 4.3C: Current

The Quanta SEM imposes some restrictions on beam currents. The current is a function of beam spot size, which ranges from 1-7 in steps of  $\frac{1}{2}$ . This is practically a current range between about 40 pA to 1.8 nA. For patterning purposes, a member of the research group used a Faraday cup and a Keithley 6487 Pico ammeter to measure the beam current for each spot size at least once a month. Though the beam current corresponding to any spot size can fluctuate quite significantly over time, all structures on which resistivity measurements were performed for this work were fabricated within a

week of one another, and thus it can be assumed that the current remained relatively constant across each sample.

In order to see a trend between resistivity and current, deposition was performed across three different beam currents, 457 pA, 524 pA, and 866 pA. The dose for each sample was held constant at 100  $\mu\text{C}/\text{cm}^2$  and was delivered across 5 loops. The purity for each current was also determined in order to isolate any effect to either the composition or internal deposit geometry.

Gas EBID studies have previously shown that a higher beam current results in a lower resistivity deposit, as illustrated by this literature review [9]. It is thought that the higher beam energy could be having an annealing effect. As no parametric study has been done on the resistivity relative to beam current, it was initially theorized they would have the same relationship. As it was expected that any changes in resistivity would result from deposition grain size, purity was not anticipated to vary between the beam currents used.

#### 4.3D: Annealing

As described in Section 3.4, thermal annealing has been shown to result in significant reductions in resistivity for both high purity electroplated copper and low purity copper deposited via EBID. Considering previous results have shown the resistivity of LP-EBID deposited copper remaining an order of magnitude higher than those of bulk, annealing could result in a significant reduction [21]. Due to the relatively high metal content in copper deposited via LP-EBID compared to gas phase deposits, it is

expected that annealing will not result in the same dramatic change in volume. However, the reduced impurities would also suggest that the reductions in resistivity would not be as great. With the purity of LP-EBID deposited copper falling between that of previously studied electroplated copper and gas phase EBID copper, it is hypothesized that the relative reduction in resistivity will be as well. That is, that the resistivity will be significantly reduced, but not by an order of magnitude after thermal annealing.

#### 4.4: Annealing Parameters

Based on the work described in section 3.4, samples were annealed for 20 minutes at a maximum temperature of 300 degrees Celsius with a ramp rate of approximately 2 degrees per second in an annealing furnace at CENSE. Due to equipment limitations, the deposits were annealed in air.

#### 4.5: Cross Section Procedure

All cross sections referenced in this work were performed on a Helios Nanolab 660, manufactured by FEI Co. The samples were coated first with EBID deposited platinum and then platinum deposited via ion beam to protect them during the cross sectioning process. Once the cross section was completed, EDX images were taken at a 52-degree tilt to determine the internal composition of the structures.

#### 4.6: Resistance Measurement

All resistivity measurements referenced in this work were performed using a probe station manufactured by Cascade Microtech working with a Keithley 2400 Sourcemeter both provided by the UK Center for Nanoscale Engineering (CeNsE). Measurements where simply checking for conductivity was all that was required were conducted using only a two-point probe across the inner two pads, while all resistance measurements were carried out with the four-point method. Given values are an average, using Microsoft Excel, of the slope between 5 current measurements ranging from 10-50 mA in equal steps of 1 mA, with a compliance voltage of 100 mV. The only exceptions were the first two four points measurements and the circuit edit attempt, which were performed at Cypress Semiconductor under lower current conditions. Using a standard four-point probe setup, the current was forced through the outer two pads while voltage was measured across the inner two to calculate the resistance values. This is illustrated in Figure 10, below. Once the average resistance was obtained, the resistivity could be calculated using the dimensions measured via ESEM and Equation 2, below.

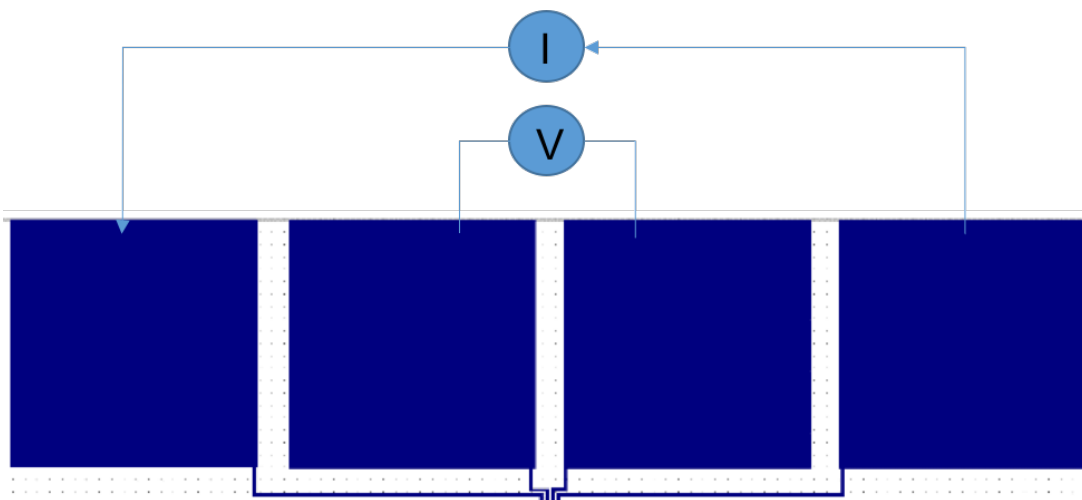


*Figure 10 Four Point Probe Method [21]*

$$\textit{Resistivity} = \textit{Resistance} * \frac{\textit{Cross Sectional Area}}{\textit{Length}}$$

Equation 2: Resistance to Resistivity Conversion

## 5: Results

### 5.1: Early Circuit Edit Work

One of the primary potential applications of LP-EBID is in the area of circuit edit/debug. Thus far, research in LP-EBID has focused primarily on studying the mechanisms of deposition, increasing purity, and improving control over the liquid. There has, as of yet, been no practical demonstration of LP-EBID's ability to edit a real circuit. In order to achieve a demonstration, one of the early focuses of this work was to use LP-EBID to repair an existing IC.

The circuit edit work was accomplished using a wafer provided by Cypress Semiconductor. As this was a first attempt, it was decided to focus on the test structures located in the upper metal layers of the chip, as these would be both easy to access, edit and measure. Thus, the structure chosen was a four-point probe pattern in the top layer of the chip. The 8-inch wafer was much too large to fit in the temperature controlled stage on the Quanta. So, it was diced into 5x5 mm sections, centered on the desired structures, by American Dicing Inc. The unedited structure can be seen in Figure 11 (A).

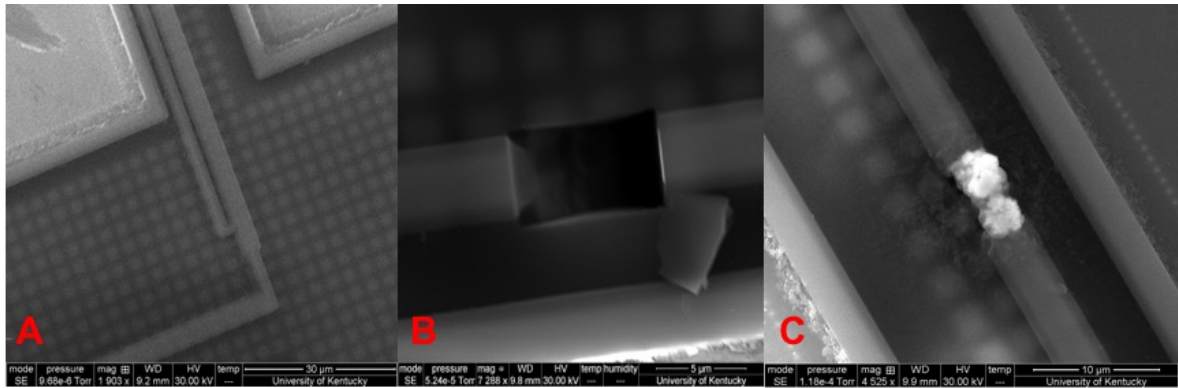


Figure 11 (A) Unedited Test Structure (B) Sectioned Removed via Helios Dual-Beam (C)

*Patch implemented via LP-EBID*

Once the wafer was diced, a 5  $\mu\text{m}$  section of the desired structure was removed using a Helios Electro/Ion Dual Beam System, manufactured by FEI Company, as seen in Figure 11 (B). The sample was then transferred to the FEI Quanta where deposition was performed. The deposition process was very similar to that for patterning copper nanowires, described in Section 4.2. The initial line was patterned along the center of the gap, at a current of 461 pA and a dose of 250  $\mu\text{C}/\text{cm}$  for a length of 7 $\mu\text{m}$ , to ensure connection on both sides of the 5 $\mu\text{m}$  gap. Once the initial line was deposited, a reduced area scan was run, with the area covering the entire gap region. This induced deposition in the remaining liquid precursor, resulting in deposits of the kind seen in Figure 11 (C). Once deposition was completed and imaging ensured a visible connection, the four point probe structure was measured at Cypress Semiconductor using the procedure previously described in Section 4.5

*Table 5: Resistance Comparison of Test Structures*

<b>Sample</b>	<b>Resistance</b>
<b>Pre-Edit</b>	8.5 $\Omega$
<b>Open Circuit</b>	196.6 k $\Omega$
<b>Patched</b>	52.2 k $\Omega$

Despite the visible connection in high vacuum imaging and proven conductivity of deposits formed under similar conditions, the resistance was five orders of magnitude above that of the previously measured structure. As can be seen in Table 5, the resistance of the patterned structure was only a factor of four less than the open circuit created by milling.

In order to determine the cause of the incredibly high resistance, one of the deposits was cross sectioned using the Helios Dual-Beam system and then analyzed via energy-dispersive X-ray spectroscopy (EDS). This allowed the elemental composition of the deposit to be easily determined, as well as allowing for continuity to be verified deeper in the structure. As can be seen in Figure 12 (A), the structure was continuous across the entire gap. Additionally, as can be seen in Figure 12 (B), significant copper deposits are also continuous across the entire gap.

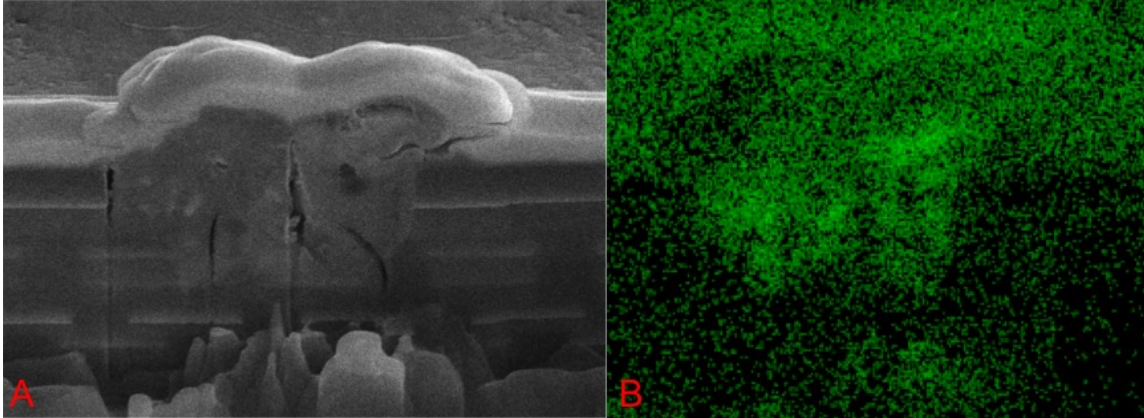


*Figure 12 (A) Cross Section of Deposit (B) Copper Content in Deposit*

Once continuity and relative purity were verified via cross section, other potential issues could be considered. While the deposit was copper, the interconnects on the test structure were aluminum. Though there should be no issues with conductivity between the two metals, it is thought that the exposure to air, between milling on the Helios and deposition on the Quanta, resulted in the formation of a thin layer of aluminum oxide ( $\text{Al}_2\text{O}_3$ ). It has long been established that aluminum oxide can form a self-limiting film several nanometers thick within minutes of exposure to air at room temperature [33]. While was not initially considered to be a barrier to attempts to edit the circuit, it is now believed that editing the aluminum circuit with copper deposition in two separate chambers is an impossibility. Another possibility is that the dose effect, described in section 5.2, also caused issues with the contact.

## 5.2: Effect of Dose

In order to improve the patterning success rate, the initial sample set for this study was patterned entirely at a high dose ( $100\text{-}250 \mu\text{C}/\text{cm}$ ), and as mentioned in section

4.3C, one loop for the current variation to reduce grain size. All 12 samples in this initial set measured resistances beyond the ability of both the Cypress Semiconductor and CeNsE probe stations to measure, effectively an open circuit. This prompted extensive investigation as to the cause of the issue.

The only differences between the new samples and previous work were the test structures used and, realized later, the dose used in deposition. Deposition of platinum test structures via gas phase EBID was performed across the leads of the probe structures, as can be seen in Figure 13 (A), below. Measurement with the CeNsE probe station confirmed their functionality. In order to check for the presence of an insulating barrier, platinum patches were deposited across the top of the copper nanowire to attempt to circumvent this as can be seen in Figure 13 (B). However, the patched structures remained effectively non-conductive. This led to the hypothesis that the dose was somehow playing a greater role than anticipated in the patterning process and that the issue was with the composition of the deposits.

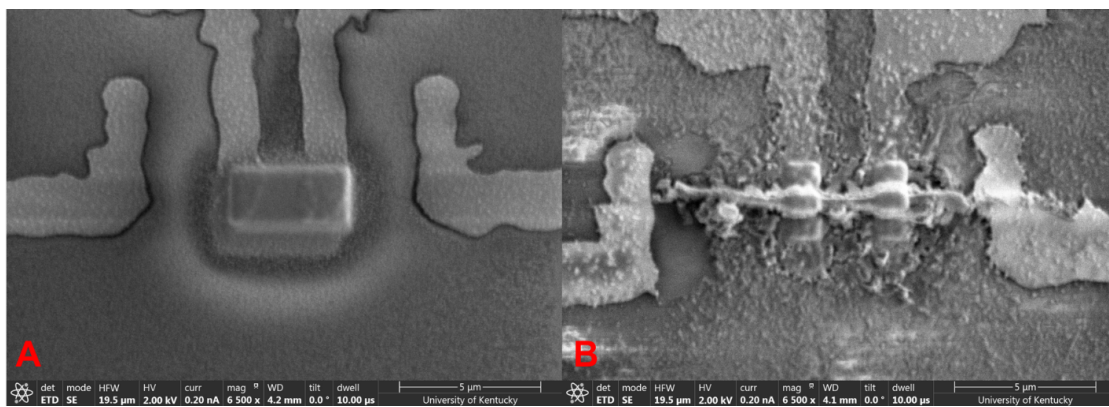


Figure 13 (A) Platinum Test Structures for Two Point Measurement (B) Patched Copper

### Nanowires

Initial structures patterned at low doses measured as conductive. It should be noted that in this case, a two-point probe was used to verify connection. The difference

between the samples is incredibly stark and using only a two-point probe allowed for faster fabrication of more data to explore the effect of dose.

As can be seen in Figure 14 there is a strong trend between the total dose and the number of loops used in the deposition process. This trend can be better visualized in Figure 15, which shows a clear cutoff between 20 and 25  $\mu\text{C}/\text{cm}$  per patterning loop. Syam's samples are also featured to illustrate previous work relative to these results.

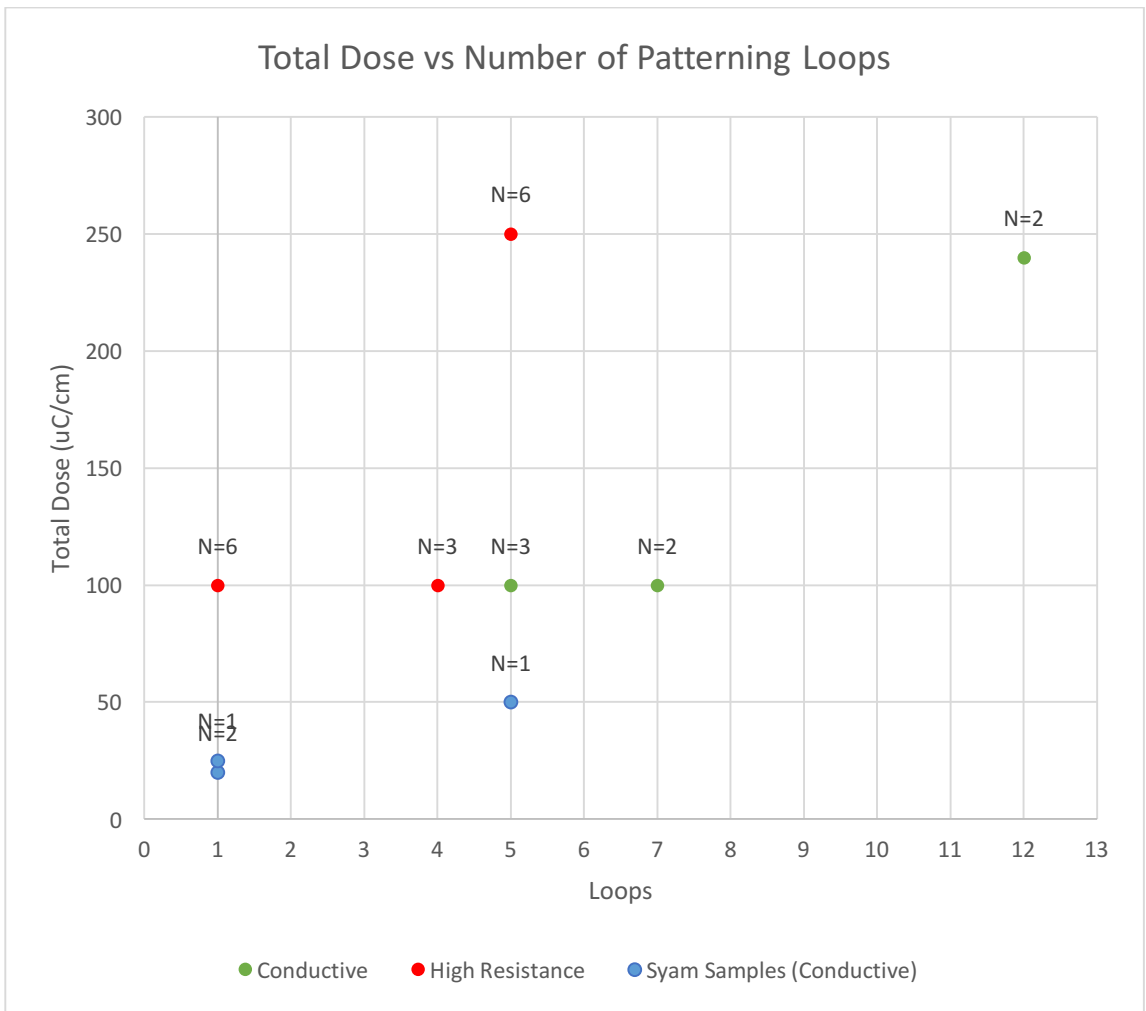
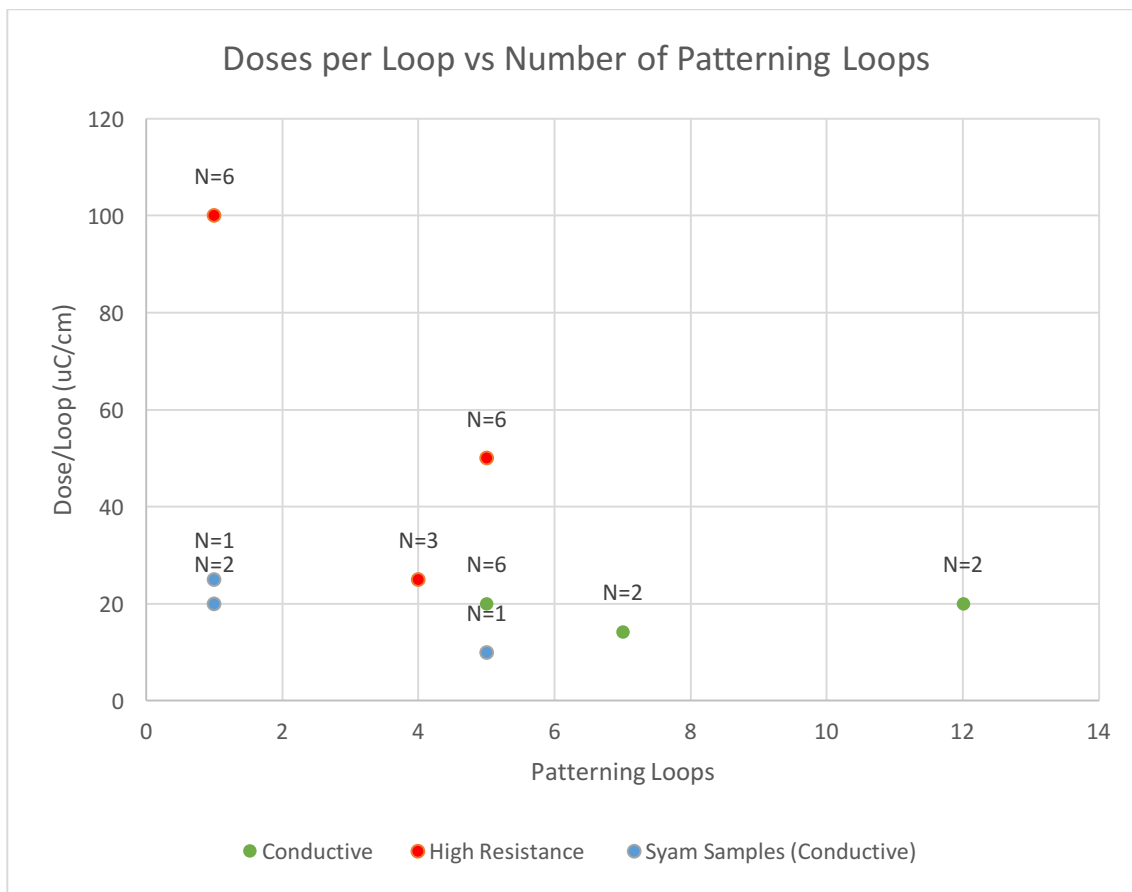


Figure 14: Total Dose vs Number of Patterning Loops



*Figure 15 Dose per Loop vs Number of Patterning Loops*

Despite the massive difference in conductivity, there appears to be no correlation between the exterior qualitative appearance of the deposit and the dose/loop. This can be observed in Figure 16 A and D below. It should be noted that the additional collateral deposition is thought to be the result of liquid thickness and not the use of loops.

However, cross section reveals that the internal structure to be quite different. As can be seen in Figure 16 B and E, the single loops structure is extremely porous, despite a continuous exterior appearance. By contrast, the looped deposit is solid and possesses visible copper grains. EDX analysis also revealed the two structures differed somewhat in material composition. As can be seen in Figure 16 C and F, the looped deposit also shows

a high quantity of copper compared to the single loop. Averaged values for the purity are provided in Table 6. It is worth noting the significant silicon and oxygen present in the surrounding material that are likely interfering with the reading. Due to the presence of oxygen in the SiO<sub>2</sub> substrate, it was not included in the Table. The values presented are intended as a relative comparison only and not a quantitative assessment of deposit purity. The values for both the porous and non-porous areas of the non-conductive structure are included.

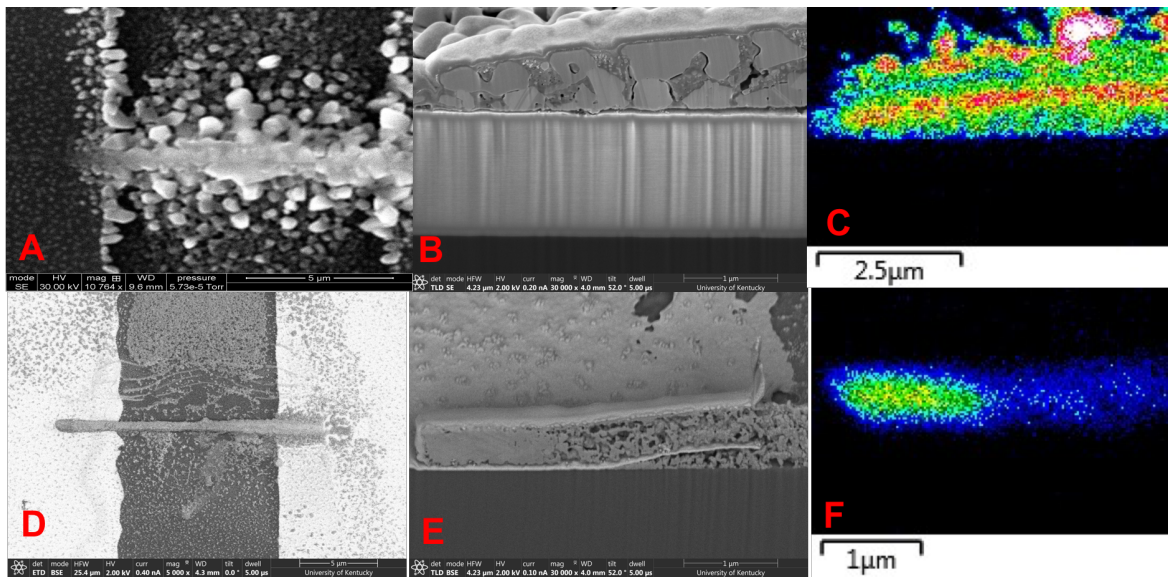


*Figure 16 (A) Looped Sample Top Down View (B) Looped Sample Cross Section (C) Looped Sample Copper Content (D) Non-Looped Sample Top Down (E) Non-Looped Sample Cross Section (F) Non-Looped Sample Copper Content*

*Table 6 Looped vs Non-Looped Copper Content*

Sample	Copper Atomic Weight Percentage
<b>Looped</b>	85%
<b>Non-Looped Porous</b>	15%
<b>Non-Looped Non-Porous</b>	34%

### 5.3: Effect of Beam Current

Qualitatively the nanowires patterned at three different beam currents do not appear to vary significantly from one another, as can be seen in Figure 17, below. A and C appear somewhat similar, compared to B, but these were the most separated in terms of beam current.

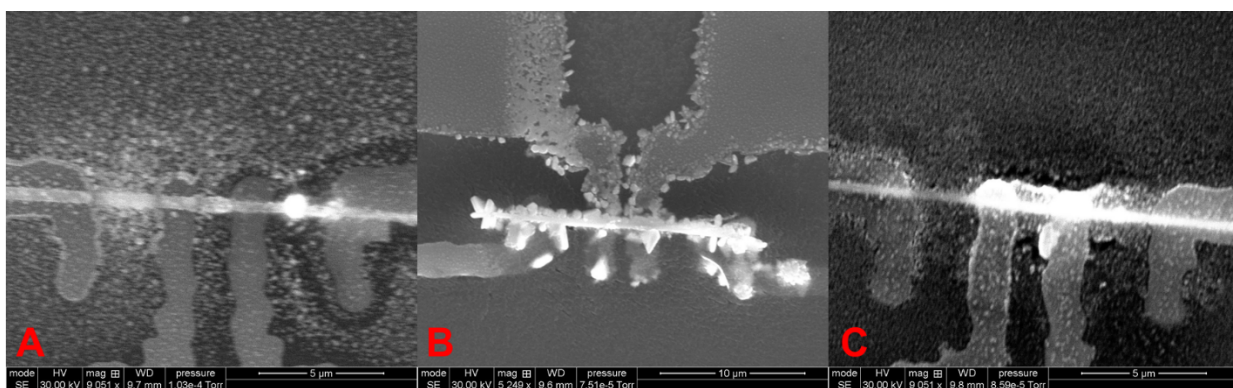


*Figure 17 (A) Nanowire patterned at 259 pA (B) Nanowire Patterned at 524 pA (C)*

*Nanowire Patterned at 866 pA*

There was also no measured trend in resistivity with beam current, as can be seen in Figure 18, below. The quantitative values measured can be found in Table 7. It should be noted that Syam's samples differ in total dose and the dose/loop, as is referenced in in

the table and these are denoted in the sample name. It should be noted that measurement error in the dimensions could result in a 10% error on either side, however this is negligible compared to the observed process variability.

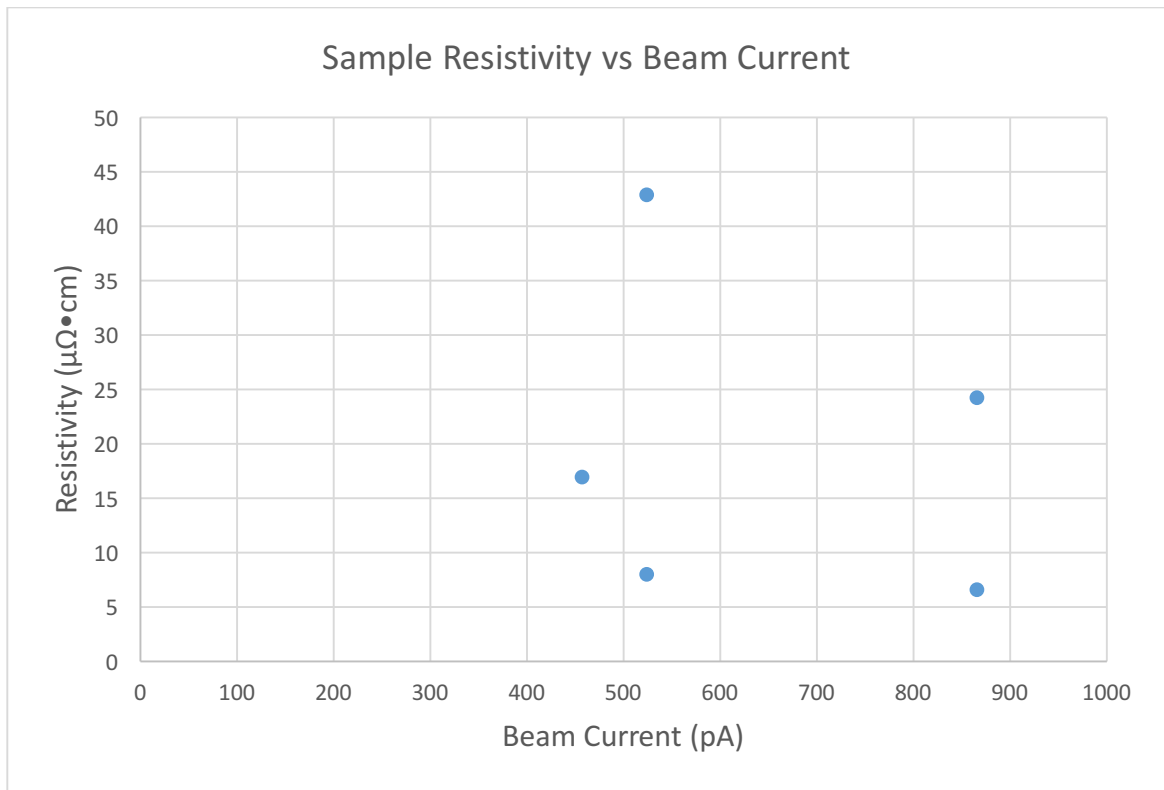


*Figure 18 Sample Resistivity vs Beam Current*

*Table 7 Smith and Syam Resistivity Data*

Sample	Beam Current (pA)	Total Dose ( $\mu\text{C}/\text{cm}$ )	Dose per Loop ( $\mu\text{C}/\text{cm}$ )	Resistivity ( $\mu\Omega\cdot\text{cm}$ )
<b>Old 4.0-D3</b>	457	100	20	2500
<b>Old 4.0-D14</b>	457	100	20	17
<b>4.0-UL</b>	524	100	20	8
<b>4.0-LR</b>	524	100	20	43
<b>4.5-UR</b>	866	100	20	6.6
<b>4.5-LR</b>	866	100	20	24
<b>Syam-A</b>	550	25	25	5000
<b>Syam-B</b>	550	20	20	800
<b>Syam-C</b>	683	20	20	370
<b>Syam-D</b>	1286	50	10	67

As can be seen in the raw data, achieved resistivity in all samples produced for this work was lower than anything recorded previously for any EBID process. It should be noted that sample Old 4.0-D3 was excluded from the graph as it suffered significant contamination prior to measurement, as is elaborated in the discussion section. However, there is no reliable trend with beam current. Indeed, the data does not even seem to be reliable on this scale for deposits fabricated under identical conditions. Despite their differences in resistivity, there is very little visible difference in the nanowires. As can be seen in Figure 19 below.

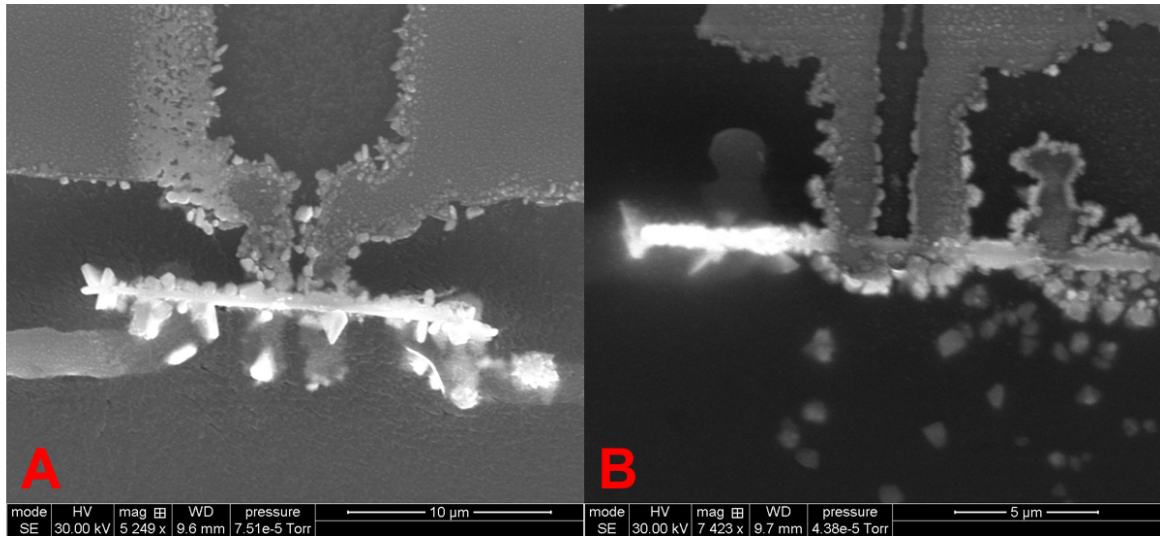


*Figure 19 (A) Structure 4.0-UL, Lower Resistivity (B) Structure 4.0-LR, Higher Resistivity*

#### 5.4: Effect of Annealing

Annealing of the deposits resulted in a significant visual change and a total loss of conductivity. As can be seen in Figure 20, below. Significant additional material appears to have grown around the original nanowire. This result is likely due to oxidation of the copper deposits after having been exposed to and high temperatures, as was feared would happen.

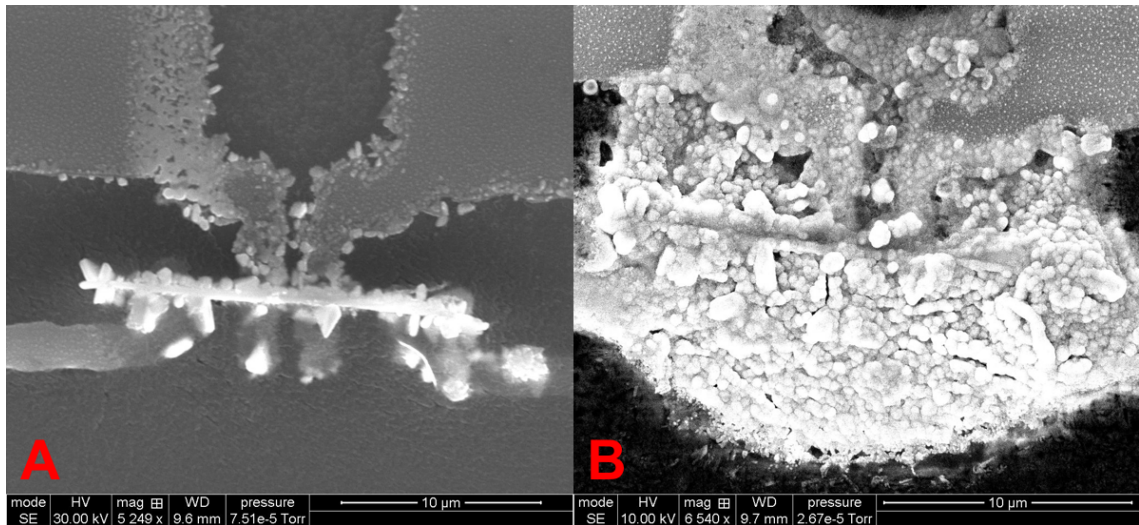
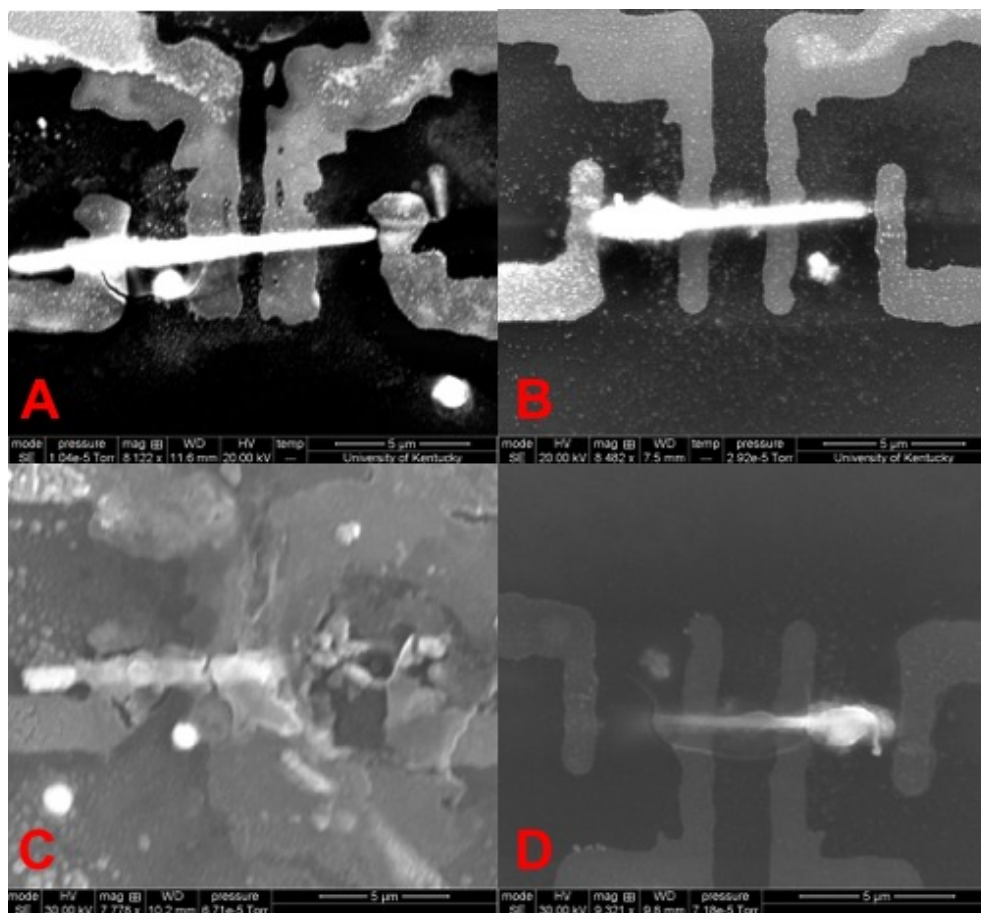


Figure 20 (A) Deposit before Annealing (B) Deposit After Annealing

### 5.5: Sample Degradation Over Time

Due to equipment issues and the generally low success rate of the deposition process for this work, there were often long periods of time between the initial fabrication of samples and their measurement. It was noted that over time many samples appeared to degrade quite drastically. In many cases the structure would virtually vanish. However, in most cases, it would appear visibly weathered but still partially intact, as can be seen in Figure 21 Below. The upper images show the samples immediately after fabrication, in October of 2017, while the lower images were taken in March of 2018.



*Figure 21 (A) Sample 1 Imaged in October 2017 (B) Sample 2 Imaged in October 2017*

*(C) Sample 1 imaged in March 2018 (D) Sample 2 imaged in March 2018*

It can be seen, particularly in A and C, that there is significant precursor residue remaining on the sample. In many cases, the sample was not cleaned due to adhesion issues with the probe leads. While the deposits themselves would sometimes be removed in a post cleaning step with DI water, this generally correlated with the strength of the deposit, which in turn generally correlated with the total dose and beam current used. The primary issue was with the probe leads. As can be observed in Figure 22, below, the leads would often lose adhesion during the deposition process and then be removed from the

deposit by the rinse. The lead that was rinsed away left a clear outline in the collateral deposition on the sample, and took a piece of the copper deposit with it.

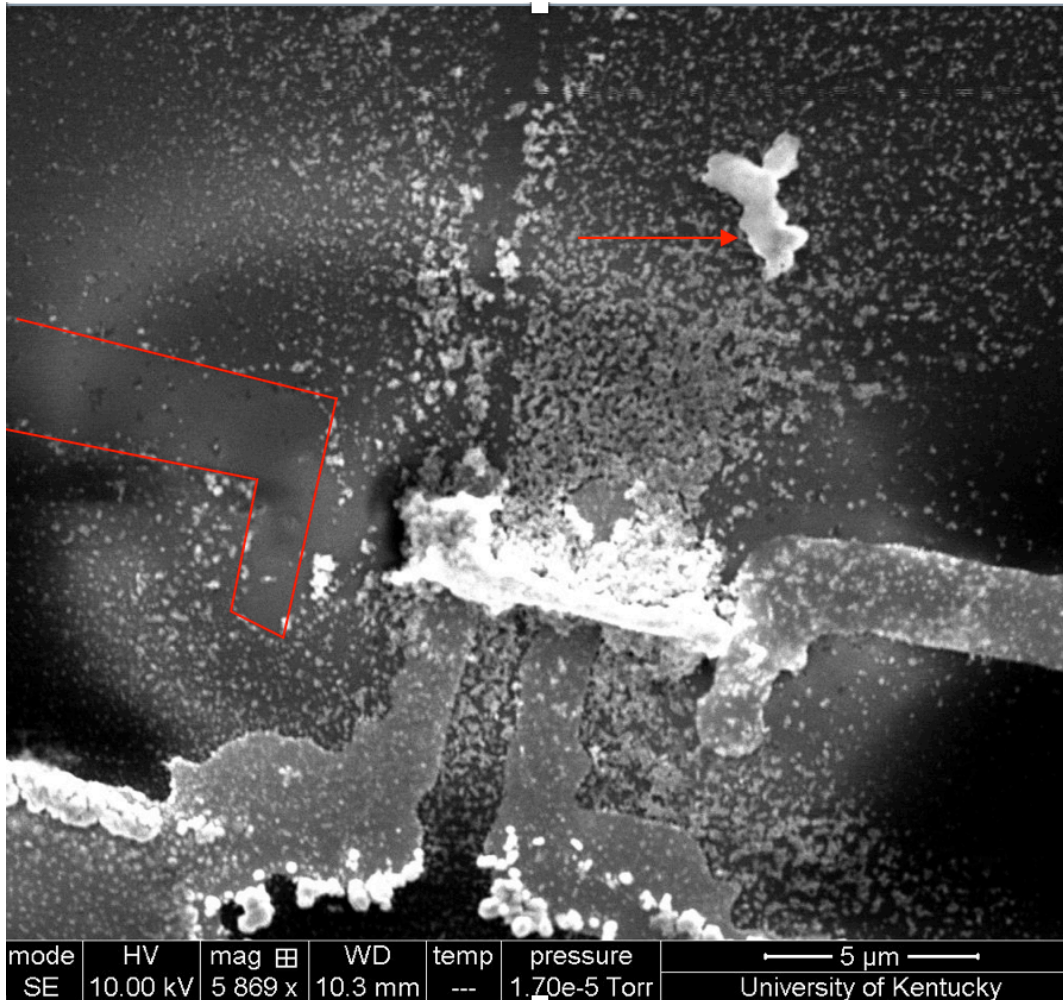


*Figure 22 Probe Lead Loss of Adhesion, Former Location of Probe Lead and Section of Copper Deposit Removed are Annotated*

As the degradation did not occur in samples that were rinsed, the issue is likely being caused by the precursor remaining on the substrate. Since this is only composed of copper sulfate and sulfuric acid for all experiments, it seems that the sulfuric acid is the

most likely source of the deposit degradation. While sulfuric acid has been demonstrated as an etchant for copper via Liquid Phase Electron Beam Induced Etching (LP-EBIE), it is known to not spontaneously etch copper [34]. The leads were only vulnerable to loss of adhesion after going through the deposition process, which suggests the chromium adhering the gold to the  $\text{SiO}_2$  is also being affected.

In order to ascertain if spontaneous etching of copper by sulfuric acid was even possible, a quick experiment was conducted. 1  $\mu\text{m}$  of copper was electrodeposited on a 1.7  $\mu\text{m}$  thick  $\text{SiO}_2$  substrate. A drop of a 5M solution of sulfuric acid was then placed on top of this for 24 hours. As can be seen in Figure 23 below, significant etching did occur. While the method of deposition and chemical composition of LP-EBID deposits is certainly different than that of electrodeposited copper, it illustrates the potential for sulfuric acid to be involved in the degradation of the copper deposits over time if not removed immediately after patterning.

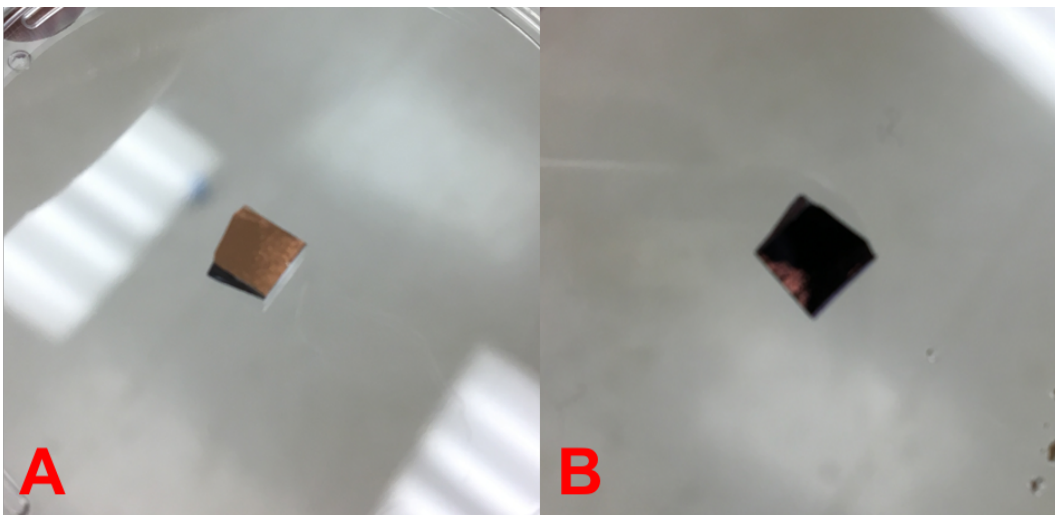


*Figure 23 (A) Copper Sample before acid exposure (B) Copper Sample after 24 of exposure to 5M Sulfuric Acid*

## 5.6: Discussion

Each of the previously presented results will be discussed in depth and explanations for the observed effects will be presented. No discussion is given on Section 5.5, as no quantitative data was collected and it presented merely an observation.

### 5.6A: Effect of Dose

As can be observed in the results presented, the dose per loop plays a critical role in determining the effectiveness of this process. The measured samples indicate a very narrow range, between 20 and 25  $\mu\text{C}/\text{cm}$  of dose per loop where the samples move from being incredibly conductive to effectively non-conductive. The exception to this is one result produced by Syam, which measured as conductive at one loop of 25  $\mu\text{C}/\text{cm}$  [21]. During the measurements conducted for this work, some samples were also measured beyond the apparent dose cutoff of 25  $\mu\text{C}/\text{cm}$ .

The porous nature of the structure, revealed via cross section, may offer an explanation for these anomalies. Despite the very low density and copper content, it is possible for a conductive pathway to exist through the porous sections of the nanowire, albeit with a much lower probability than a looped structure. It can be theorized that it is not an instantaneous and absolute switch from good to poor conductivity, but rather a drastically reduced probability of a viable conductive pathway through the structure.

As far as explaining the porous structure itself, the most likely explanation is that depletion of copper within the precursor. When the total dose is delivered in a single loop, the beam spends much longer paused over each location it steps to. It is possible the available copper is being depleted very rapidly upon beam exposure, leaving little material left to deposit for the rest of the dwell time in a specific area. When the dose is looped, the copper content at each location along the line can replenish before being exposed to the beam.

This conclusion can be further supported by the geometry of the deposit seen in Figure 16 (E). The structure appears to be much denser, and measured a much greater copper content, at the beginning and the end of the pattern. At either end, there are many more directions from which the precursor could replenish the exposed area than at the center, where it could only enter from either side. This is illustrated by Figure 24, below.

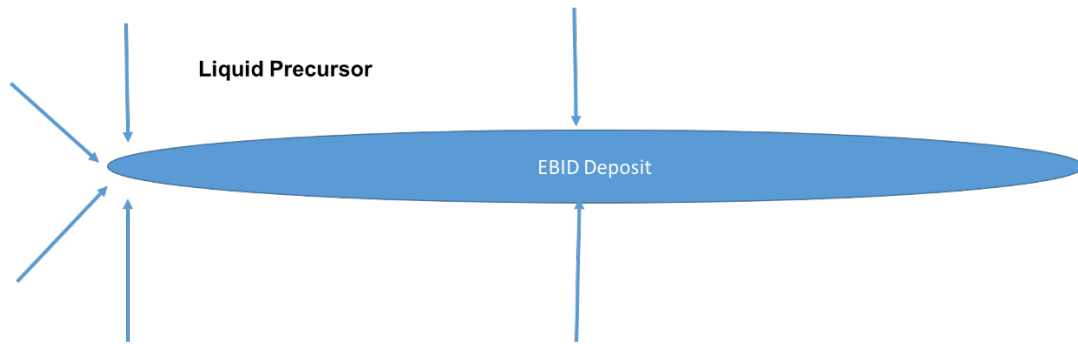


*Figure 24 Available Paths of Precursor Replenishment*

However, if the availability of copper in the liquid precursor is indeed decreasing as the beam dwells longer over a specific location, it is interesting that the volume of the deposit does not change. That is, if there is less material available for deposition why is the resulting structure not simply smaller rather than less dense. It is likely that some

other material is forming in the open spaces of the structure during the deposition process. This could be oxidized copper, which is very rapidly removed by the sulfuric acid during the deposition process. It could also be either hydrogen or oxygen gas, which becomes trapped inside the deposit. Either case is very difficult to pin down via cross sectional EDX and considering the high resistivity regardless of the material creating the pores significant investigation is likely not warranted.

#### 5.6B: Effect of Current

Even with only two beam currents, the spread of data between them and at each point supports the conclusion that the beam current used has no effect on the resistivity of resulting structures. The lowest resistivity achieved for this work was  $6.5 \mu\Omega\cdot\text{cm}$ , which is only a factor of 4 higher than the bulk value for copper of  $1.7 \mu\Omega\cdot\text{cm}$ . All structures referenced were lower than the best previous result of  $67 \mu\Omega\cdot\text{cm}$  [21].

The one outlier, denoted as sample Old 4.0-D3 in section 5.3 is likely so much higher than the others due to contamination. The probe leads were lost due to the adhesion issues mentioned in section 5.5, and the structure was reattached via EBID deposited platinum in the Helios Nanolab, as can be seen in Figure 25 below. While the four-point probe removes contact resistance, it is very likely that, being that close to the deposition, significant contamination was introduced to the deposit.

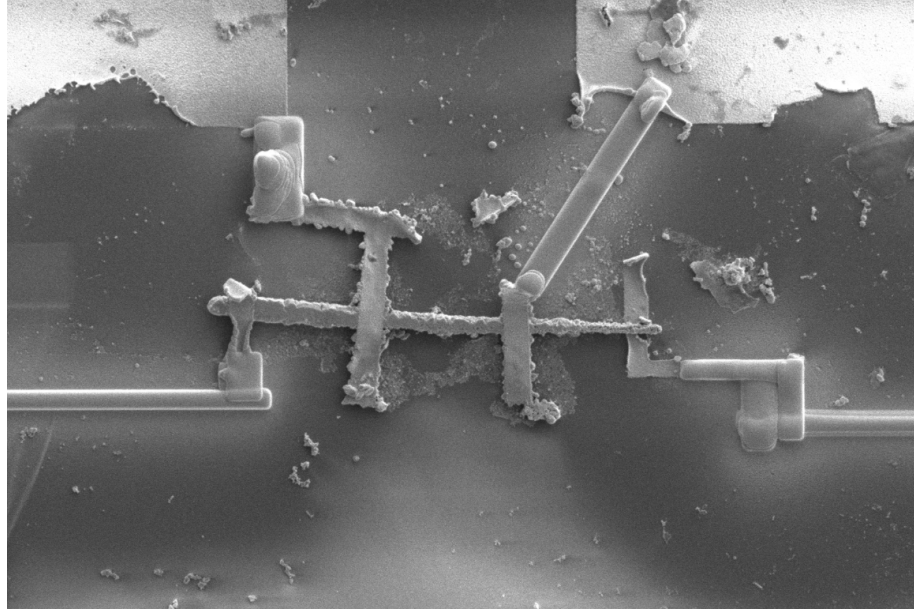


*Figure 25: Probe Lead Repair Via Ion Deposition of Platinum*

As illustrated in Table 7, all measured values were significantly lower than any of those measured by Syam. There are several possible explanations for this. The most likely is that he was experimenting with several different additives, all of which have been shown to lower the purity of the resulting deposit [21] [8]. His highest resistivity sample was also exposed to the Ion beam during platinum deposition, further supporting the hypothesis that contamination may have vastly increased the resistivity. Finally, he was consistently using a lower total dose than any used in this work. His lowest resistivity sample used a higher dose and a lower dose per loop. Further quantitative investigation is necessary to investigate the role of either of these parameters on resistivity.

## 6: Conclusion

### 6.1: Future Work

Completing this work has highlighted the challenges and research directions that must be tackled to improve the LP-EBID process. Some of these areas have been discussed in detail below.

#### 6.1A: Liquid Control

The greatest challenge to the LP-EBID process is the liquid control. The thickness of the liquid at the deposition site has a greater impact on the pattern quality and success rate than any other factor. The temperature and pressure control afforded by working with the FEI Quanta is insufficient to reliably pattern in localized areas with a reasonable success rate. Though efforts to modify the precursor have certainly improved the ease of the LP-EBID technique, other avenues could be pursued to improve the process. Without even a reliable way to measure the liquid thickness, it is difficult to isolate the effect of any other variable from the film thickness at the working site.

#### 6.1B: Collateral Deposition Reduction

The formation of collateral deposition does not qualitatively appear to relate to either looping or beam current. During this work it has also not been observed to correlate with increasing total dose. In a practical application, the presence of such

collateral could damage surrounding structures and in any case, it significantly reduces the achievable resolution of the LP-EBID process. It can be guessed that the liquid film thickness at the patterning site plays a dominant role in the formation of such collateral depositions. However, the work of Esfandiarpour, et al, demonstrated that the precursor composition also plays a role [8]. Further study is necessary to isolate precisely what variables influence such deposition and mitigate them as much as possible.

#### 6.1C: Further Parametric Investigation

The revelation that the dose/loop, a variable previously thought to have no effect, could impact the patterning process so greatly highlights how much there is still to learn about the mechanics of the LP-EBID process. It is clear that assumptions carried over from gas phase work cannot be assumed to be true for work with liquid precursors. Thus it becomes important to conduct further parametric investigation into the many variables that affect the process. If there were a reliable method to measure the liquid thickness, a quantitative study of the effect of thickness on pattern reliability and resistivity would be most beneficial. Further work on the dose/loop and total dose using four point samples could provide quantitative data on if additional loops have an impact on resistivity. Other variables, such as dwell time, accelerating voltage, beam current, and precursor concentration could also be examined to determine their effect on resistivity.

## 6.1D: Circuit Edit Applications

The discovery of the significant effect of dose per loop on the resistivity of the resulting deposit suggests that the issues encountered with the early circuit edit work presented here may have been the result of the copper deposit and not aluminum oxide formation, as was previously assumed. Many samples, already diced, remain from the ship provided by Cypress Semiconductor and their resistance before editing has already been measured. It would be a relatively easy project to once again mill a gap into the connection and replace it with LP-EBID deposited copper, this time using a lower dose per loop and no reduced area scans to ensure a reliable connection.

## 6.2: Conclusion

In conclusion, this work has demonstrated that copper can be deposited with high accuracy and purity, allowing for applications in circuit edit, debug, and rapid prototyping. It was discovered that the dose per loop plays a significant role in the resistivity of copper deposited via LP-EBID, with a drop from high conductivity to effective non-conduction occurring between doses of 20 and 25  $\mu\text{C}/\text{cm}$ . A dose per loop higher than this resulted in a porous structure, likely due to the depletion of copper within the liquid precursor.

No correlation was found between the beam current used for deposition and the resulting resistivity of the deposits. However, resistivity was demonstrated to be lower

than any value previously recorded for copper nanowires deposited via LP-EBID. The lowest resistivity achieved in this work, without post-processing, was  $6.5 \mu\Omega\cdot\text{cm}$ , which is only a factor of 4 above the bulk resistivity of copper which is  $1.7 \mu\Omega\cdot\text{cm}$ .

## References

- [1] Leonidas E. Ocola, Chad Rue , and Diederik Maas, "High-resolution direct-write patterning using focused ion beams," *MRS BULLETIN*, vol. 39, pp. 336-341, April 2014.
- [2] a. J. M. Anthony J. DeMarco, "Contact resistance of focused ion beam deposited platinum and tungsten films to silicon," *Journal of Vacuum Science & Technology B*, vol. 19, no. 8, pp. 2543-2546, 20 8 2001.
- [3] Yann-Wen Lan, Wen-Hao Chang, Yuan-Chih Chang, Chia-Seng Chang and Chii-Dong Chen, "Effect of focused ion beam deposition induced contamination on the transport properties of nano devices," *Nanotechnology*, vol. 26, no. 1, pp. 1-5, 15 1 2015.
- [4] A Botman, J J L Mulders and CW Hagen, "Creating pure nanostructures from electron-beam-induced deposition using purification techniques: a technology perspective," *Nanotechnology*, vol. 20, pp. 1-17, 26 8 2009.
- [5] IA. Luisier, I. Utke, T. Bret, F. Cicoira, R. Hauert, S.-W. Rhee, P. Doppelt, and P. Hoffmann, "Comparative Study of Cu Precursors for 3D Focused Electron Beam Induced Deposition," *Journal of The Electrochemical Society*, vol. 151, no. 8, pp. 535-537, 2 7 2004.
- [6] D. a. Hastings, "Electron-Beam-Induced Deposition of Platinum from a Liquid Precursor," *Nano Letters* , vol. 9, no. 7, pp. 2715-2718, 1 June 2009.
- [7] Ilya I. Tumkin, Vladimir A. Kochemirovsky □, Mikhail D. Bal'makov, Sergey V. Safonov, Elvira S. Zhigley, Lev S. Logunov, Ekaterina V. Shishkova " *Surface & Coatings Technology*, no. 265, pp. 187-192, 2 10 2014.
- [8] Samaneh Esfandiarpour, Lindsay Boehme and J Todd Hastings, "Focused electron beam induced deposition of copper with high resolution and purity from aqueous solutions," *Nanotechnology*, vol. 28, no. 12, pp. 1-14, 21 2 2017.
- [9] W. F. van Dorp, and C. W. Hagen, "A critical literature review of focused electron beam induced deposition," *Journal of Applied Physics*, vol. 104, no. 081301, 2008.
- [10] "N. Silvis-Cividjian, C. Hagen, P. v. d. Kruit, M. vd Stam, and H. Groen," *APPLIED PHYSICS LETTERS*, vol. 92, no. 20, pp. 3514-3516, 19 5 2003.
- [11] H. W. P. Koops, A. Kaya, and M. Weber, "Fabrication and characterization of platinum nanocrystalline material grown by electron-beam induced deposition," *Journal of Vacuum Science and Technology* , vol. 13, no. 461, 1995 .
- [12] K. T. Kohlmann-von Platen, L.-M. Buchmann, H.-C. Petzold, and W. H. Brünger, "Electron-beam induced tungsten deposition: Growth rate enhancement and applications in microelectronics," *Journal of Vacuum Science and Technology* , vol. 10, no. 6, pp. 2690-2694, 1992.
- [13] Mostafa M. Shawrav, Philipp Taus, Heinz D. Wanzenboeck, M. Schinnerl, M. Stöger-Pollach, S. Schwarz, A. Steiger-Thirsfeld & Emmerich Bertagnolli, "Highly conductive and pure gold nanostructures grown by electron beam induced deposition," *Scientific Reports* , vol. 6, September 2016.

- [14] G. Schardein, E. U. Donev and J. T. Hastings, "Electron-beam-induced deposition of gold from aqueous solutions," *Nanotechnology*, vol. 22, no. 015301, pp. 1-6, 6 12 2010.
- [15] L. E. Ocola, A. Joshi-Imre, C. Kessel, B. Chen, J. Park, D. Gosztola and R. Divan, "Growth characterization of electron-beam-induced silver deposition from liquid precursor," *Journal of Vacuum Science & Technology B*, no. 30, p. 6, 2012.
- [16] M. Bresin, A. Chamberlain, E. U. Donev, C. B. Samantaray, G. S. Schardien and J. T. Hastings, "Electron-Beam-Induced Deposition of Bimetallic Nanostructures from Bulk Liquids," *Angewandte Chemie International Edition*, no. 52, pp. 8004-8007, 2013.
- [17] M. Bresin, B. R. Nadimpally, N. Nehru, V. P. Singh and J. T. Hastings, "Site-specific growth of CdS nanostructures," *Nanotechnology*, vol. 24, no. 50, 2013.
- [18] Steven J. Randolph, Aurelien Botman and Milos Toth, "Capsule-free fluid delivery and beam-induced electrodeposition in a scanning electron microscope," *Royal Society Advances*, no. 43, pp. 20016-20023, 21 11 2013.
- [19] Jeffrey S. Fisher, Peter A. Kottke, Songkil Kim,† and Andrei G. Fedorov "Rapid Electron Beam Writing of Topologically Complex 3D Nanostructures Using Liquid Phase Precursor," *Nano Letters*, 16 10 2015.
- [20] Matthew Bresin, Aurelien Botman, Steven J Randolph, Marcus Straw, and Jeffrey Todd Hastings, "Liquid Phase Electron-Beam-Induced Deposition on Bulk Substrates Using Environmental Scanning Electron Microscopy," *Microscopy and Microanalysis*, vol. 20, pp. 376-384, 3 1 2014.
- [21] A. Syam, "Electron Beam Induced Deposition of Highly Conductive Copper Nanowires from Bulk Liquids," University of Kentucky, Lexington, 2017.
- [22] Aleksandra Szkudlarek, Alfredo Rodrigues Vaz, Yucheng Zhang, Andrzej Rudkowski, Czesław Kapusta, Rolf Erni, Stanislav Moshkalev and Ivo Utke, "Formation of pure Cu nanocrystals upon post-growth annealing of Cu–C material obtained from focused electron beam induced deposition: comparison of different methods," *Beilstein journal of nanotechnology*, vol. 6, pp. 1508-1517, 2015.
- [23] Yograj Singh Duksh, Brajesh Kumar Kaushik, Sankar Sarkar, Raghuvir Singh,, "Performance comparison of carbon nanotube, nickel silicide nanowire and copper VLSI interconnects: Perspectives and challenges ahead," *Journal of Engineering, Design and Technology*, vol. 8, no. 3, pp. 334-353, 2010.
- [24] J. Tao, N. W. Cheung, and C. Hu,, "Electromigration characteristics of copper interconnects," *IEEE Electron Device Letters*, vol. 14, pp. 249-251, 1993.
- [25] S.Y. Lee, N. Mettlach, N. Nyguyen, Y.M. Sun, and J.M. White, "Copper Oxide Reduction Through Vacuum Annealing," *Applied Surface Science*, no. 2003, pp. 102-109, 2003.
- [26] Samantha G. Rosenberg, Michael Barclay, and D. Howard Fairbrother, "Electron Induced Surface Reactions of Organometallic Metal(hfac)<sub>2</sub> Precursors and Deposit Purification," *Applied Materials and Interfaces*, vol. 6, no. 11, p. 8590–8601, 2014.
- [27] M. Stangl, and M. Militzer, "Modeling self-annealing kinetics in electroplated Cu thin films," *Journal of Applied Physics 1*, vol. 103, 2008.

- [28] Jin Onuki\*, Kunihiro Tamahashi, Takashi Namekawa and Yasushi Sasajima, "Effect of Additive-Free Plating and High Heating Rate Annealing on the Formation of Low Resistivity Fine Cu Wires," *Materials Transactions* , vol. 52, no. 9, pp. 1818-1823, 2011.
- [29] J. J. Plombon, Ebrahim Andideh, Valery M. Dubin, and Jose Maiz, "Influence of phonon, geometry, impurity, and grain size on Copper line resistivity," *Applied Physics Letters* , vol. 89, 2006.
- [30] Aleksandra Szkudlarek, Alfredo Rodrigues Vaz, Yucheng Zhang, Andrzej Rudkowski, Czesław Kapusta, Rolf Erni, Stanislav Moshkalev and Ivo Utke, "Formation of pure Cu nanocrystals upon post-growth annealing of Cu–C material obtained from focused electron beam induced deposition: comparison of different methods," *Beilstein Journal of Nano Technology* , vol. 2015, no. 6, p. 1508–1517, 13 7 2015.
- [31] S.-C. Chang, J.-M. Shieh, B.-T. Dai and M.-S. Feng, "Reduction of resistivity of electroplated copper by rapid thermal annealing," *Jorunal of the Electrochemical Society* , vol. 5, no. 6, pp. C67-C70, 6 2002.
- [32] Jin Onuki, Kunihiro Tamahashi, Takashi Namekawa and Yasushi Sasajima, "Impact of High Heating Rate, Low Temperature, and Short Time Annealing on the Realization of Low Resistivity Cu Wire," *Materials Transactions* , vol. 51, no. 9, pp. 1715-1717, 2010.
- [33] M. H. a. P. Fowle, "Naturally and Thermally Formed Oxie Films on Aluminum," *JOURNAL OF THE ELECTROCHEMICAL SOCIETY* , vol. 103, no. 9, pp. 482-485, 9 1956.
- [34] Lindsay Boehme, Matthew Bresin, Aurélien Botman, James Ranney and J Todd Hastings "Focused electron beam induced etching of copper in sulfuric acid solutions," *Nanotechnology*, vol. 26, 20 10 2015.
- [35] Bresin, M.; Chamberlain, A.; Donev, E. U.; Samantaray, C. B.; Schardien, G. S.; Hastings, J. T, "Electron-Beam-Induced Deposition of Bimetallic Nanostructures from Bulk Liquids\*\*," *Nanoparticles* , vol. 52, pp. 8004-8007, 2013.

## Vita

Gabriel William Smith

### Education

Masters/Bachelor of Science in Electrical Engineering, minor in Mathematics

University of Kentucky, Lexington, KY

Bachelor GPA: 3.75/4.0

Masters GPA: 4.0/4.0

### Positions Held

University of Kentucky, First Year Engineering Teaching Assistant

University of Kentucky, Graduate/Undergraduate Researcher

Kentucky Industrial Assessment Center, Intern

### Honors

Member of Tau Beta Pi

Member Eta Kapp Nu

Dean's List

Cosgriff Award